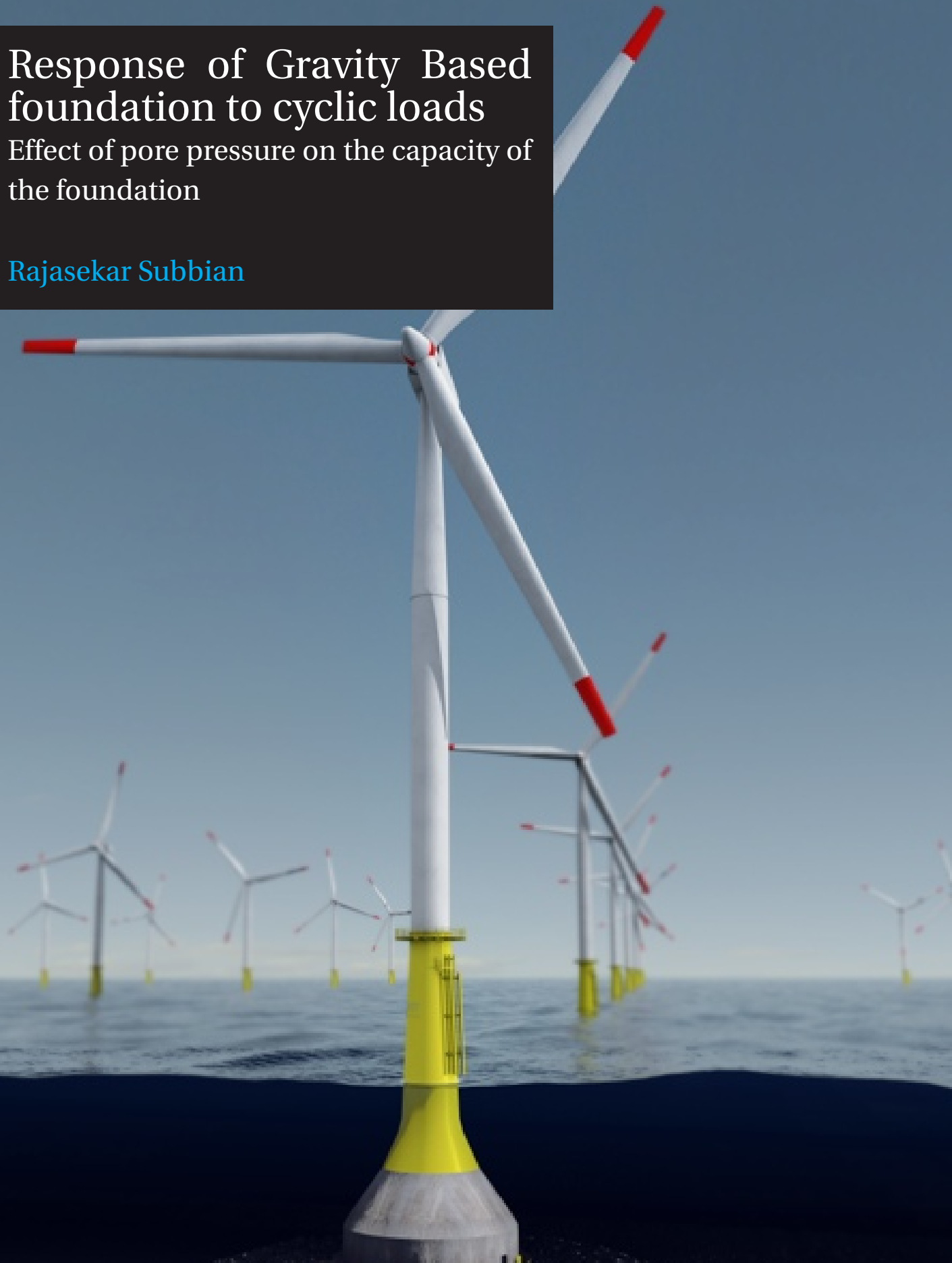


Response of Gravity Based foundation to cyclic loads

Effect of pore pressure on the capacity of the foundation

Rajasekar Subbian

Technische Universiteit Delft



RESPONSE OF GRAVITY BASED FOUNDATION TO CYCLIC LOADS

EFFECT OF PORE PRESSURE ON THE CAPACITY OF THE
FOUNDATION

by

Rajasekar Subbian

in partial fulfilment of the requirements for the degree of

Master of Science

in Civil Engineering with specialisation in Geo-engineering

at the Delft University of Technology,
to be defended publicly on Tuesday, November 28, 2017.

Supervisor:	Prof. dr. K. G. Gavin	TU Delft
Thesis committee:	dr. F. Pisano,	TU Delft
	Ir. K. Reinders,	TU Delft
	Ing. P. van Ogtrop,	Witteveen+Bos
	dr. L. J. Prendergast,	TU Delft

This thesis is confidential and cannot be made public until November 28, 2017

An electronic version of this thesis is available at <http://repository.tudelft.nl/>.

Cultivation of mind should be the ultimate aim of human existence.- Dr. B.R. Ambedkar

ABSTRACT

The development in harvesting trend of wind energy is evidenced as a result of the Paris convention. Therefore, future wind turbines tend to move towards deeper water, which sets a requirement of larger capacity support structure. The design guidelines of Gravity Based Foundation (GBF) which is capable of supporting deeper water wind turbines lack attention on the cyclic response of the foundation.

The undrained capacity of GBF in terms of failure envelope under combined loading is investigated numerically, in order to shed light on the effect of cyclic loads on the capacity of the foundation. A GBF supporting a 5 MW wind turbine on sandy soil domain is designed based on the static conditions. A critical state model called Hypoplastic sand model with intergranular strain concept is adopted to represent the soil domain in 2D. The influence of factors such as relative density (D_r), load characteristics (τ_{cyc} & τ_{avg}) and the wave frequency on the pore pressure behaviour are analysed in the event of concluding a critical case. Moreover, it should be noted that the number of cycle is restricted to 50 cycles as a result of limitations in the implicit method.

An undrained failure envelope is developed for the critical case, which in comparison with original envelope reveals the expansion in undrained capacity with respect to the number of cycles. It is inferred that the expansion in the capacity is because of the process known as densification which overcomes the effect of pore pressure on the failure envelope. It is also worth noting that the consolidation phase which is used to model the loads has a significant influence on the expansion of the failure envelope.

ACKNOWLEDGEMENTS

This report is the result of graduation thesis for my Master of Science degree in Geo-Engineering at Delft University of Technology and Witteveen+Bos.

I would like to thank all the members of my graduation committee and Witteveen+Bos for offering this thesis to me. I would like to thank Luke for making himself available whenever I approached him with doubts. Without his inspirations, the accomplishment of this thesis would not have been possible. I would also like to thank my committee members Ken, Federico and Kristina for their valuable comments about my progress during all the review meetings. In particular, I would like to thank Pal for his invaluable comments on my PLAXIS models. Moreover, I would like to thank my beloved brothers JP and AP for helping me understand the critical concepts of Finite Element Modelling. I am also obliged to thank my brothers Sathish, Markus, Krishnamoorthy, Vinoth, and my fellow students of Geo-Engineering for their help during my thesis. Finally, I express my gratitude to my family and friends who always supported me during my ups and downs.

*Rajasekar Subbian
Delft, November 2017*

CONTENTS

Abstract	v
List of Figures	xi
List of Tables	xiii
1 Introduction	1
1.1 Offshore wind energy	1
1.2 Foundations	2
1.2.1 Monopiles	2
1.2.2 Gravity Based Foundations (GBF)	2
1.2.3 Suction caisson foundation	2
1.3 Aim of the research	2
1.4 Limitations	3
1.5 Sign conventions	3
1.6 Structure of the research	4
2 Literature Review	5
2.1 Loading Conditions	5
2.2 Design Basis	6
2.2.1 Bearing Capacity	6
2.2.2 Sliding resistance	8
2.2.3 Settlement calculation	8
2.2.4 Dynamic response	10
2.2.5 Soil strength degradation	11
2.3 Response of the foundation to cyclic loading	13
2.4 Base case of Gravity Based Foundation	15
2.4.1 Loads on the offshore wind turbine	15
2.4.2 Gravity Based Foundation dimensions	16
2.4.3 Failure envelope under combined loading	17
2.5 Advanced constitutive models	18
2.5.1 Elastoplasticity models	18
2.5.2 Hypoplasticity models	20
2.5.3 Hybrid models	24
2.6 Factors influencing the cyclic behaviour of the soil	24
2.7 Conclusion	25
3 Finite element modelling of the Gravity Based Foundation and the soil domain	27
3.1 Foundation	27
3.2 Constitutive model	28
3.3 Loading strategy	28
3.3.1 Methodology 1	28
3.3.2 Methodology 2	30
3.4 Mesh dependency	30
3.5 Initial and Boundary conditions	31
3.5.1 Initial conditions	31
3.5.2 Boundary conditions	32
3.6 Factors influencing the cyclic behaviour of the soil	32
3.6.1 Relative density	32
3.6.2 Load characteristics	33
3.6.3 Wave frequency	33

3.7	Conclusion	33
4	Analysis and Results	35
4.1	General Description.	35
4.1.1	Stress conditions.	35
4.1.2	Stress points	35
4.2	Stress behaviour	36
4.2.1	Pore pressure behaviour	36
4.2.2	Total stress behaviour	38
4.3	Influence of factors on cyclic behaviour of the soil	38
4.3.1	Influence of relative density on cyclic behaviour	38
4.3.2	Influence of load characteristics on cyclic behaviour.	39
4.3.3	Influence of wave frequency on cyclic behaviour	40
4.4	Capacity of the foundation	41
4.4.1	Liquefaction potential	41
4.4.2	Failure envelope of the foundation in H-M space under combined loading	42
4.4.3	Influence of cyclic behaviour of soil on H-M failure envelope	43
4.4.4	Influence of time period in consolidation on the failure envelope	44
4.5	Conclusion	44
5	Conclusions and Recommendations	47
5.1	Conclusions.	47
5.1.1	Sub-question 1.	47
5.1.2	Sub-question 2.	48
5.1.3	Main question	49
5.2	Recommendations	49
A	Appendix	51
A.1	Wind load.	51
A.2	Wave load.	51
A.2.1	Design wave height and wave period.	52
A.2.2	Wave length	52
A.2.3	Wave particle kinematics.	52
A.2.4	Morison equation	53
B	Appendix	57
B.1	Base case foundation dimension	57
B.2	Bearing capacity	57
B.3	Sliding Resistance.	58
B.4	Rotational check	58
C	Appendix	61
D	Appendix	63
D.1	Relative density	63
D.2	Load characteristics.	63
D.3	Wave frequency.	63
	Bibliography	67

LIST OF FIGURES

1.1	Developments and capacity in wind energy	1
1.2	Sign convention used in this research	3
1.3	Structure of the research	4
2.1	Wind turbine subjected to different loads and their transmission to the foundation[1]	6
2.2	Effective area of the eccentrically loaded circular loading	7
2.3	Pictorial representation of sliding failure mechanism	8
2.4	Graph from DNV [2] to find bearing capacity factors and modulus number	9
2.5	The influence of the base plate stiffness on stress distribution with respect to depth	10
2.6	Excitation frequency range for offshore wind turbine (Prendergast et al, 2015 [3])	11
2.7	Maximum horizontal hydrodynamic load resulting in the foundation	16
2.8	Geometry of the gravity based foundation used in this thesis	17
2.9	Failure envelope of the foundation under combined loading in static condition	17
2.10	Failure surface generated under working vertical load	18
2.11	Shape of different yield surfaces [4]	20
2.12	Failure criterion comparison between Mohr-coulomb and matsuoaka-nakai criteria (Matsuoka & Nakai (1985))[5]	21
2.13	Measurement of angle of repose [6]	22
2.14	Determination of n and Compression curve showing the influence of n and h_s on them [6]	22
2.15	Relation between void ratio e and pressure p_s [6]	23
2.16	Determination of parameter α and β [7]	23
3.1	Simplified geometry of the foundation	28
3.2	Loading strategy and the resulting settlement	29
3.3	Loading pattern used in this analysis	30
3.4	The generated mesh used in this analysis	31
3.5	The boundary conditions for the soil domain used in this analysis	32
4.1	Anticipated stress state around the foundation [8]	35
4.2	Stress points chosen for this analysis	36
4.3	Pore pressure generated during each phase	37
4.4	Pore pressure behaviour on medium dense sand ($D_r=53\%$)	37
4.5	Total stress behaviour on medium dense sand ($D_r=53\%$)	38
4.6	The development of failure surface	39
4.7	Pore pressure behaviour with respect to relative density	39
4.8	Pore pressure behaviour with respect to load characteristics	40
4.9	Pore pressure behaviour with respect to wave frequency	40
4.10	The potential for liquefaction failure at different stress points below the foundation	41
4.11	Failure envelope of our foundation in H-M space	42
4.12	Failure surface generated under working vertical load	42
4.13	Failure surface experienced by Gournvec a)toppling (scoop) b) wedge-scoop-wedge [9]	43
4.14	Effect of cyclic load on the capacity of the foundation	43
4.15	Comparison of failure envelopes	44
A.1	Particle orbit in accordance with Airy theory [10]	53
A.2	Water particle velocity and acceleration in horizontal direction at the still water level	53
A.3	Mac camy-Fuchs correction for the inertia coefficient C_m [11]	54
A.4	Inertial and drag forces resulting from morison equation	54
A.5	Maximum horizontal hydrodynamic load resulting in the foundation	55

B.1	Base case foundation used in this analysis	57
D.1	Pore pressure behaviour with respect to relative density	64
D.2	The influence of load characteristics on pore pressure behaviour in response to cyclic loads	65
D.3	The influence of frequency on pore pressure behaviour in response to cyclic loads	66

LIST OF TABLES

2.1	Loads without considering the design factors used in the preliminary design	15
2.2	The permanent load of a 5 MW wind turbine including the foundation	15
2.3	Parameters used for the load calculation (both wind and wave)	16
2.4	Parameters of hypoplastic sand model	21
3.1	Parameters of the foundation plate	27
3.2	Model parameters of the Hostun sand	28
3.3	Factor of safety depending on the coarseness factor	31
3.4	Magnitude of cyclic load (τ_c) for the wave frequency 0.1 Hz subjected by various parts of the foundation	33
B.1	Step by step calculation for the bearing capacity	58
B.2	Step by step calculation for the sliding resistance	58
B.3	Step by step calculation for the rotational check	58
C.1	Drainage type investigation	62

NOMENCLATURE

p	Total principle stress [kPa]
p_s	Average limit value of p [kPa]
α	Exponent [-]
α	Parameter that helps in finding the steepness of the cap [-]
$\bar{\gamma}, \gamma'$	Average unit weights above and below the foundation level, respectively [kN/m^3]
Δu	Change in pore pressure resistance [kN/m^2]
δ	Settlement in Z direction [m]
$\Delta\sigma_d$	Change in deviatoric stress [kN/m^2]
$\Delta\sigma_d$	Deviatoric stress [kN/m^2]
$\Delta\sigma_m$	Change in mean total stress [kN/m^2]
$\Delta\theta(n)$	Change in accumulated rotation during cyclic loading [-]
\dot{T}	Objective stress rate tensor
\dot{u}	Water particle acceleration [m/s^2]
γ'	Effective submerged unit weight [kN/m^2]
\hat{T}	Natural period of the system [s]
$\hat{T} = T(t)$	Granulate stress ratio tensor
λ	Wave length [m]
ν	Poisson's ratio [-]
ϕ	Interface friction angle [$^\circ$]
ϕ'	Effective friction angle [$^\circ$]
$\phi'_{initial}$	Initial friction angle of sand [$^\circ$]
ϕ'_{red}	Reduced friction angle of sand [$^\circ$]
ϕ_d	Design friction angle [$^\circ$]
ϕ_m	Mobilised friction angle [$^\circ$]
ϕ_p	Peak friction angle [$^\circ$]
ϕ_{cv}	Friction angle at critical state [$^\circ$]
Π_1	Dimensionless number [-]
ρ	Density of the air [kg/m^3]
ρ_s	Density of the soil [kg/m^3]
ρ_w	Density of water [kg/m^3]

ρ_{water}	Density of water [kg/m^3]
σ'	Effective stress in the layer [kPa]
$\sigma'_1, \sigma'_2, \sigma'_3$	Major, intermediate and minor principle effective stresses, respectively [kN/m^2]
$\sigma_1, \sigma_2, \sigma_3$	Major, intermediate and minor principal stresses, respectively [kN/m^2]
σ_a	Reference stress (100kPa) [kPa]
τ_{avg}	Average shear stress [kN/m^2]
τ_{cyc}	Cyclic shear stress [kN/m^2]
θ_s	Accumulated rotation during monotonic loading [-]
ε	Strain in Z direction [-]
ζ	Wave amplitude [m]
ζ_b, ζ_c	Load characteristics [-]
A	Rotor swept area [m^2]
a	Stress dependency exponent [-]
A_{eff}	Effective Area [m^2]
B	Foundation breadth [m]
b_{eff}	Effective breath [m]
c	Cohesion [kN/m^2]
c'	Effective cohesion [kN/m^2]
C_c	Secant compression index [-]
C_d	Drag coefficient [-]
c_d	Design cohesion [kN/m^2]
C_m	Inertia coefficient [-]
C_T	Thrust co-efficient [-]
D	Bulk modulus of the soil [kPa]
D	Deformation rate tensor
D	Dilatancy parameter [-]
D	Foundation embedment depth [m]
d	depth [m]
$d\gamma_v^p$	Plastic shear increment [-]
$d\varepsilon_v^p$	Plastic volumetric shear increment [-]
e	Void ratio [-]
e	Eccentricity [m]
e_p	Average limit value of e [-]
E_s	Young's modulus of the soil [kPa]

f_b	Barotrophy factor (stress dependency)
f_d	Pycnotrophy factor related to material state
f_e	Pycnotrophy factor (density dependency)
f_{drag}	Hydrodynamic drag load [kN/m]
$f_{inertia}$	Hydrodynamic inertia load [kN/m]
F_{thrust}	Thrust force on the wind turbine [N]
f_{achard}	Multiplier used to adjust the densification rule [-]
g	Gravity due to acceleration [m/s^2]
G_i^p	Plastic shear modulus at onset of shear mobilisation [kN/m^2]
H	Foundation influence depth [m]
H	Horizontal load [kN]
h	Dimensionless parameter [-]
H_b	Breaking wave height [m]
H_s	Significant wave height [m]
$hard$	Factor correcting densification rule for loose soils [-]
i_γ, i_q, i_c	Dimensionless inclination factors [-]
k	Permeability of the soil [m/s]
k	Stiffness [kN/m]
k	Wave number [-]
K_B^e	Elastic bulk modulus [kN/m^2]
K_f	Bulk modulus of the fluid [kPa]
K_G^e	Elastic shear modulus [kN/m^2]
k_G^p	Plasticity shear modulus [kN/m^2]
K_p	Passive earth pressure co-efficient [-]
L	Drainage length [m]
L	Stress-dependent tensor related to linear part
l_{eff}	Effective length [m]
m	Mass of the structure [kg]
m	Modulus number [-]
M_d	Factored design moment load [$kN - m$]
m_e	Elastic bulk modulus index [-]
N	Stress-dependent tensor related to non-linear part
N	Number of cycles at stress level $\Delta\sigma_d$ [-]
n	Porosity of the soil [-]

n_e	Elastic shear modulus index [-]
N_γ, N_q, N_c	Dimensionless bearing capacity factors [-]
n_{rev}	Number of shear stress reversals from loading to unloading or vice versa [-]
p'	Mean principle effective stress [kN/m^2]
p'_0	Effective overburden pressure at the level of the foundation-soil interface [kN/m^2]
p'_{ini}	Initial mean effective stress [kN/m^2]
p_A	Atmospheric pressure (100kPa) [kPa]
q	Deviatoric stress [kN/m^2]
q_d	Design bearing capacity [kN/m^2]
q_n	Uniformly distributed load [kN/m^2]
R	Radius of the foundation [m]
R_f	Failure ratio [-]
R_u	Ratio of excess pore water pressure to effective vertical stress[-]
R_u	Cumulative pore pressure resistance [kN/m^2]
S_γ, S_q, S_c	Dimensionless shape factors [-]
T	Time period of the wave [s]
T_b, T_c	Dimensionless parameters function of the load characteristics [-]
U	10 minute average wind speed at the hub level [m/s]
u	Water particle velocity [m/s]
V	Vertical load [kN]
V_d	Factored design vertical load [kN]
z	Depth of the layer [m]

1

INTRODUCTION

This chapter presents an overview of the research subject of this thesis. The ultimate objective of this chapter is to introduce the reader to the offshore wind energy industry and research questions which will be answered through the analysis.

Initially, it starts with a general introduction to offshore wind energy in Europe and emphasises their need in the current generation. Secondly, common foundation types used in supporting the offshore wind turbines are explained. Thirdly, the aim of this research is formulated as research questions. Fourthly, limitations adopted in this research are presented. Afterward, the sign convention used in this research is described. Finally, the chapter concludes with the structure of this research.

1.1. OFFSHORE WIND ENERGY

The wind was the largest interest area of the power sector in 2016 [12]. The figure 1.1 clearly shows the development in harvesting trend of wind energy until 2016. The wind energy was considered as the major driver to depart from fossil fuels and it is evidenced in figure 1.1a.

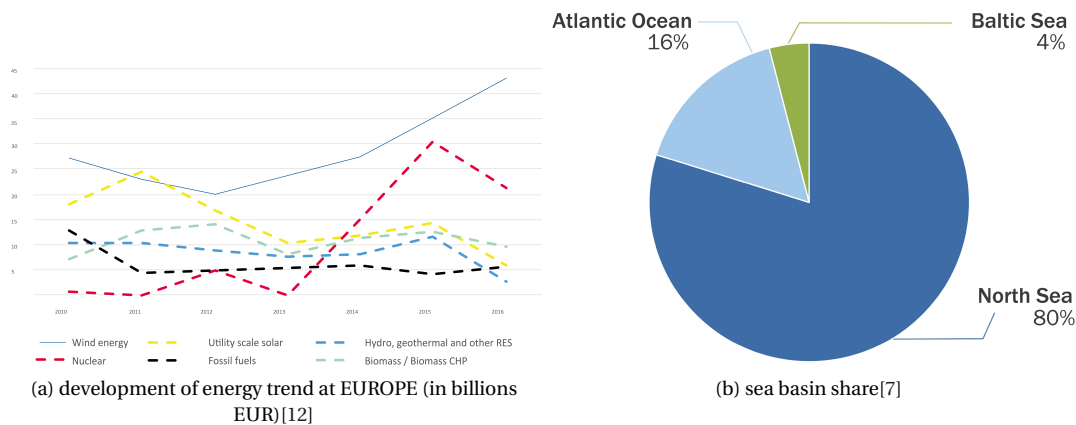


Figure 1.1: Developments and capacity in wind energy

Further, the Paris agreement on climate change highlights the importance of developing a sustainable, eco-friendly infrastructure. As a result, many countries move towards the offshore wind energy, considering the potential of it. The above figure 1.1b explicitly shows the wind energy basin share divided among the water bodies surrounding Europe. In other words, this is the geographically-described production potential of wind power. Thus, future wind turbines will move towards deeper water, where the wind speed is high. As an added advantage, the deep water turbines do not affect the aesthetics of the shore, and do not contribute to the noise pollution of nearby cities. In order to optimise the output, the turbine capacity is increased by increasing the

size of the turbine and as a result, its supporting structure. Since the cost involved in these processes are high, an optimisation can be achieved in the foundation (supporting structure) design and its installation process.

1.2. FOUNDATIONS

Foundations play a vital role in the structure by transferring loads from the superstructure to the soil domain. They vary in size and depth depending on the load and the type of the soil. The foundation design should satisfy at least two limit state requirements called as Ultimate Limit State (ULS) and Serviceability Limit State (SLS) (explained in detail in the chapter 2 [2.2]). There are several types of foundation being used for offshore wind turbines and they are as follows,

- Monopiles,
- Gravity Based Foundation, and
- Suction caissons.

1.2.1. MONOPILES

Monopile foundation also called as the deep foundation is a single pile which is driven into the sea bed to support the wind turbine. The relatively small diameter of the monopile helps it to get rid of hydrodynamic loads on a large scale. However, it also has disadvantages in deep water such as the environmental disturbance while driving it into the sea bed and the increased length which eventually increase the cost significantly, as it is made of steel. They are used in both clayey and sandy soil domain.

1.2.2. GRAVITY BASED FOUNDATIONS (GBF)

Gravity Based Foundation is a shallow foundation that makes use of the gravity load to withstand the external forces acting on the structure. It is made of concrete and is constructed onshore. In order to have larger gravity loads (higher capacity), the foundation size is increased. Although the size is increased, the installation process only involves the placement of the foundation, thus eliminating the disturbance to the environment. Unfortunately, the large size of the foundation (to have gravity loads) attracts significant hydrodynamic wave loads. It can be used in the sandy soil domain but the scour should be taken into account during the design process. In the clayey soil domain, the stability of the structure should be investigated in detail as the soil may endanger the stability of the foundation. Therefore, it requires a clear understanding of the interaction between the soil and foundation, in order to optimise the design process of the GBF. The foundation design process in accordance with current generation guidelines and the past research on them are explained in the next chapter in detail.

1.2.3. SUCTION CAISSON FOUNDATION

It is an intermediate foundation that includes advantages of both foundations (Monopiles and GBF). The installation is done in two parts namely, by gravity loads and suction. It is a relatively new foundation type which is popularly used in the clayey soil domain.

1.3. AIM OF THE RESEARCH

The ultimate aim of the research is to obtain an insight into the response of the Gravity Based Foundation capacity to the environmental loads which are cyclic in nature. Therefore, the main question is formulated as follows:

What is the effect of pore pressure (due to cyclic loads) on the capacity of the foundation?

In the event of answering it, two sub-questions have been framed as follows,

1. *How should the GBF be designed in accordance with the current generation guidelines and how the effects of cyclic loads are considered in it?*

By answering this question, the necessity of this research is realised. Furthermore, the advantage of using the failure envelope to investigate the cyclic load effects is emphasised.

2. *How do factors such as Relative density, Load characteristics of the wave and the wave frequency influence the pore pressure behaviour?*

In the event of answering this question, a critical case among the considered characteristics that is most affected by cyclic loads is figured. Thus, the failure envelope for such case can be developed in order to examine the cyclic load effects.

The pore pressure poses a serious issue in terms of stability of the structure as it directly influences the capacity of the foundation. Thus, answering these questions would pave the way to optimise the foundation design processes in the context of ULS.

1.4. LIMITATIONS

Considering the time constraint of this research, several limitations have been adopted. They are as follows:

- The cyclic load is modelled as a quasi-static load rather than as dynamic load.
- Wind load is calculated for the maximum wind speed which is a conservative assumption, whereas the wave load is calculated using a semi-empirical relation called Morison equation.
- The settlement and rotation are not focused in this research as the ultimate objective is to study the pore pressure effects on the foundation capacity.
- Soil domain is considered as homogeneous in nature which is a simplistic assumption.
- The constitutive model is calibrated with soil parameters from literature.
- The pre-design of the foundation does not take into account the dynamic loads.
- The shape of the foundation is simplified to 2D but the load application will be based on the original shape of the foundation.
- The experimental validity of the model requires future work.

1.5. SIGN CONVENTIONS

The sign convention used for input in this thesis is represented in the figure 1.2,

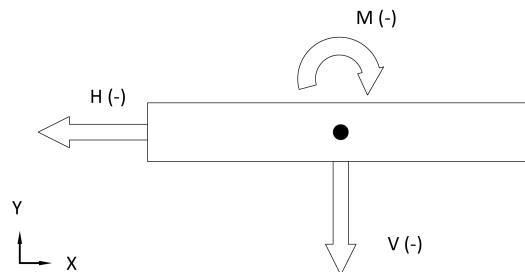


Figure 1.2: Sign convention used in this research

The sign is considered with respect to the global coordinate system for all the input. In all the output, compressive stresses and forces are considered to be negative and tensile stresses and forces are considered to be positive.

1.6. STRUCTURE OF THE RESEARCH

Main components of this research are outlined in the form of flow chart in figure 1.3. As the flow chart proceeds, the introduction is succeeded by the literature review, which would guide us in answering the sub-question 1 [1]. Following it, the finite element modelling is discussed, which in combination with the analysis and results would help in answering the sub-question 2 [2]. Eventually, the main research question would be answered based on the analysis and results. Moreover, all the answers will be summarised in the conclusion along with recommendations for future work.

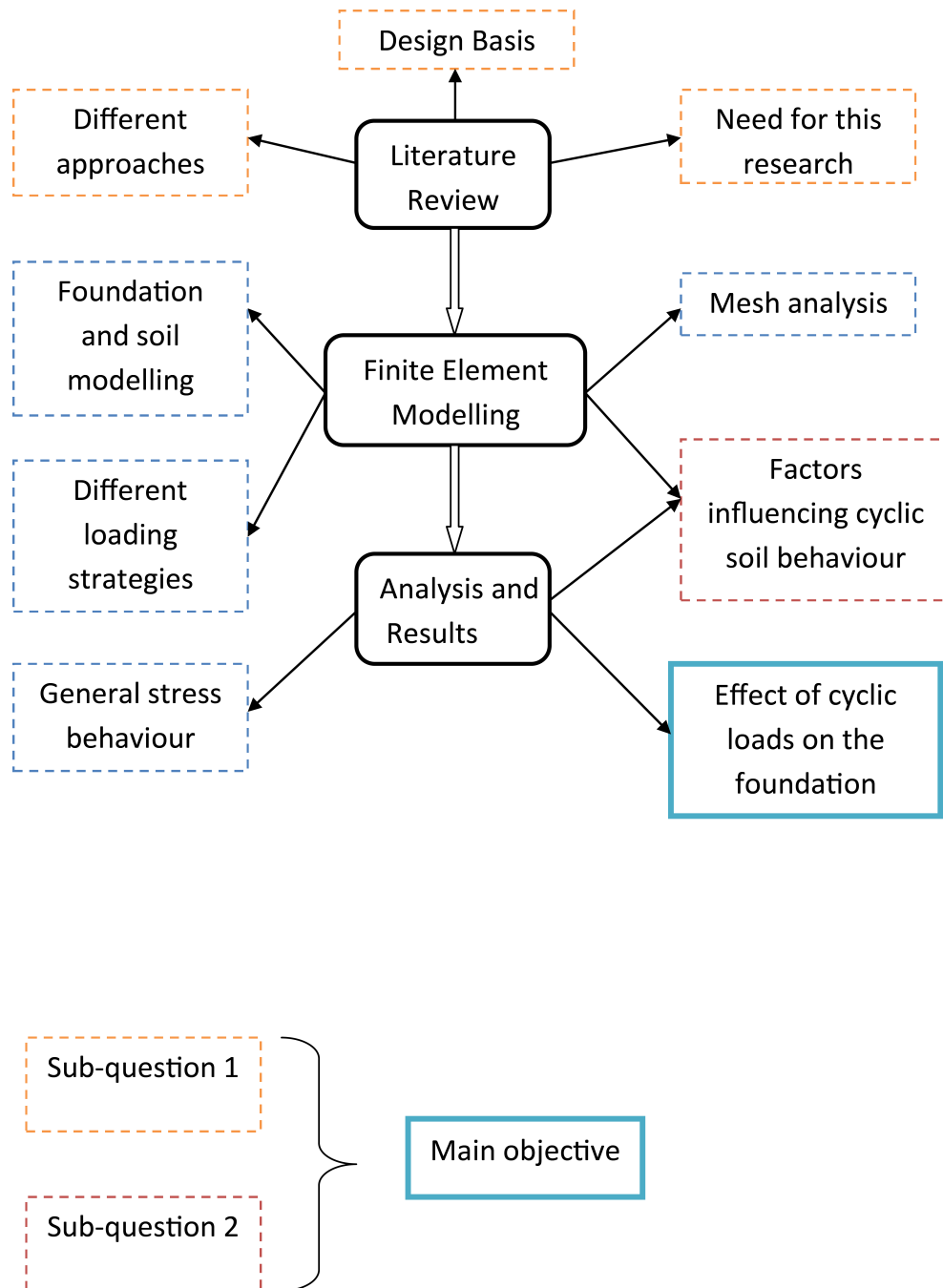


Figure 1.3: Structure of the research

2

LITERATURE REVIEW

This chapter provides an overview of the literature study carried out for this research. The objective of this chapter is to summarise the design basis of Gravity Based Foundation (GBF) according to the industrial practice, and the foundation behaviour in response to cyclic loading. Moreover, it reveals the limitations of the design practice and emphasises the necessity of this research.

Initially, it starts with relevant loads experienced by offshore wind turbines. Secondly, the design basis for the foundation design, according to the available international standards, is summarised. Thirdly, the research on the foundation response to cyclic loading and their effects on pore pressure, stiffness and settlement of the soil is presented. Following it the model foundation to be investigated in this research is presented. Penultimately, the constitutive models capable of simulating the cyclic behaviour of soils are presented. Finally, the chapter is concluded with the factors that influence the cyclic behaviour of the soil.

2.1. LOADING CONDITIONS

This section gives an insight of relevant loads to be considered for offshore wind turbines, particularly, those supported by GBS foundations. An efficient foundation design requires optimal consideration of the loads that are to be transferred by the substructure into the soil.

According to DNV [13], a wind turbine experiences various loads throughout its lifetime. Therefore, the design process should include load cases constructed by combining relevant design situations. The list of design situations and respective design loads are provided in the Table 4.1 of DNV [13]. In this research, the load due to the normal operating condition of wind turbines will be considered. Thus, accidental loads because of the ice or ship impact will not be considered. The loads considered can be classified as below,

- Permanent dead loads,

The permanent loads include the self-weight of the foundation, tower and the other components of the wind turbine, and the buoyancy due to the hydrostatic load depending on the depth of the water. Moreover, it also includes the ballast weight, which is used to increase the mass of the foundation.

- Variable environmental loads,

The variable loads to be transferred by the foundation include the loads due to both wind (aerodynamic) and wave (hydrodynamic) action. As they both act horizontally to the wind turbine, a moment is also to be considered, which will eventually result in the dominant load. This is in line with our understanding of offshore structures, subjected to higher horizontal environmental loads than vertical loads [8]. Additionally, earthquake and current induced loads also act on the wind turbine.

The environmental loads such as hydrodynamic and wind loads are considered in this research as they are the dominant cyclic loads on the wind turbine [14][15]. Especially, it can be specified that the overturning moment is dominant because of the fact that the wind load acting at the superstructure is away from the foundation base. The below figure 2.1 from Byrne(2011)[1] shows different parts of the wind turbine subjected to the above-mentioned loads and also they evidence the reaction of the whole structure to various loads.

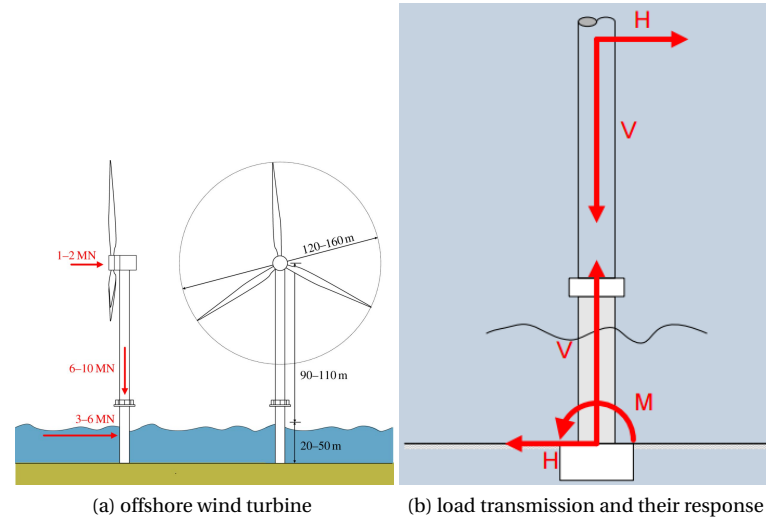


Figure 2.1: Wind turbine subjected to different loads and their transmission to the foundation[1]

2.2. DESIGN BASIS

The foundation design should be in accordance with one of the available international standards. There are two different international standards which are used for designing foundations in the offshore environment. The standards are from American Petroleum Institute (API)[16] and Det Norske Veritas (DNV) [13]. As explained in the graduation work of Lupea (2013) [7], in general, the API is recommended for the design of pile foundation and the DNV is recommended for the design of GBE. As this research is based on the GBE, DNV is considered as the standard guidelines for the design purpose. It is worth noting that the design recommendations on DNV are based on the existing guidelines of offshore platforms in oil & gas industry [17]. The difference is specified because it is well known that the overturning moment (dominant load) in the offshore wind turbine is much higher than in the oil & gas platform because of the structure height above the sea level. Therefore, the designer should have engineering judgement on the results.

The design should satisfy the limit states such as Ultimate Limit State (ULS), Serviceability Limit States (SLS), etc. which takes into account the following geotechnical issues,

- Bearing capacity,
- Stability against sliding,
- Settlements,
- Dynamic response,
- Degradation of soil strength in cyclic loading, and
- Scour.

2.2.1. BEARING CAPACITY

It is the capacity of the foundation to transfer the load into the soil and the well known Brinch Hansen equation (2.4) serves as the basis for the calculation of static bearing capacity. The equation takes into account the inclination of the load because the combination of vertical and horizontal load would result in the inclined load. As mentioned in the above section, the overturning moment plays the dominant load role which implies an eccentricity of e . Hence, the eccentricity is calculated as

$$e = \frac{M_d}{V_d} \quad (2.1)$$

where M_d and V_d are factored design moment and vertical loads respectively.

When the structure is eccentrically loaded, the effective foundation area will be reduced in accordance with

the eccentricity. Therefore, the effective foundation area is required for the bearing capacity analysis, which can be defined as

$$A_{eff} = b_{eff} * l_{eff} \quad (2.2)$$

where b_{eff} and l_{eff} are effective breadth and length respectively.

According to DNV [13], an elliptical effective foundation area can be defined for a circular foundation with radius R by the following equation,

$$A_{eff} = 2 \left[R^2 \arccos\left(\frac{e}{R}\right) - e\sqrt{R^2 - e^2} \right] \quad (2.3)$$

with major axes,

$$b_e = 2(R - e) \text{ and } l_e = 2R\sqrt{1 - \left(1 - \left(\frac{b_e}{2R}\right)^2\right)}$$

The following figure 2.2 represents the circular footing with effective foundation area marked.

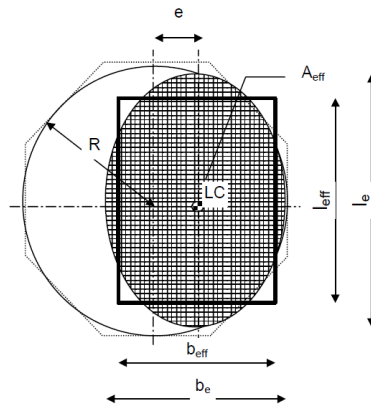


Figure 2.2: Effective area of the eccentrically loaded circular loading

The elliptical shaped effective foundation area can be represented by the rectangle with similar area as shown in the figure 2.2 with the following dimensions:

$$l_{eff} = \sqrt{A_{eff} \left(\frac{l_e}{b_e}\right)} \text{ and } b_{eff} = \left(\frac{l_{eff}}{l_e}\right) b_e$$

In the case of drained condition, the bearing capacity of the foundation with a flat base can be calculated through,

$$q_d = \frac{1}{2} \gamma' b_{eff} N_\gamma S_\gamma i_\gamma + p'_0 N_q S_q i_q + c_d N_c S_c i_c \quad (2.4)$$

where,

q_d is the design bearing capacity [kN/m^2]

γ' is the effective submerged unit weight [kN/m^2]

p'_0 is the effective overburden pressure at the level of the foundation-soil interface [kN/m^2]

c_d is the design cohesion [kN/m^2]

N_γ, N_q, N_c are dimensionless bearing capacity factors [-]

S_γ, S_q, S_c are dimensionless shape factors [-]

i_γ, i_q, i_c are dimensionless inclination factors [-]

Dimensionless factors can be calculated as

<p style="text-align: center;">bearing capacity factors</p> $N_q = e^{\alpha \tan \phi_d}$ $N_c = (N_q - 1) \cdot \cot \phi_d$ $N_\gamma = \frac{1}{4} * ((N_q - 1) \cos \phi_d)^{\frac{3}{2}}$	<p style="text-align: center;">shape factors</p> $s_\gamma = 1 - 0.4 \frac{b_{eff}}{l_{eff}}$ $s_q = s_c = 1 + 0.2 \frac{b_{eff}}{l_{eff}}$	<p style="text-align: center;">inclination factors</p> $i_q = i_c = \left(1 - \frac{H_d}{V_d + A_{eff} c_d \cot \phi_d}\right)$ $i_\gamma = i_q^2$
---	---	--

A similar procedure is followed for the undrained soil, but with different components of the Brinch Hansen equation [13]. The soil domain considered here is medium dense sand which is of much interest in North sea. Thus the behaviour is assumed to be drained in static conditions. For undrained soil like clay please refer to DNV [13].

2.2.2. SLIDING RESISTANCE

The foundation subjected to horizontal loading may tend to slide horizontally (2.3). Therefore, it is mandatory to design the foundation with sufficient sliding resistance. In the case of drained conditions, the criterion is as follows,

$$H < A_{eff} c + V \cdot \tan \phi$$

where,

H is Horizontal load [kN]

V is Vertical load [kN]

ϕ is interface friction angle [$^\circ$]

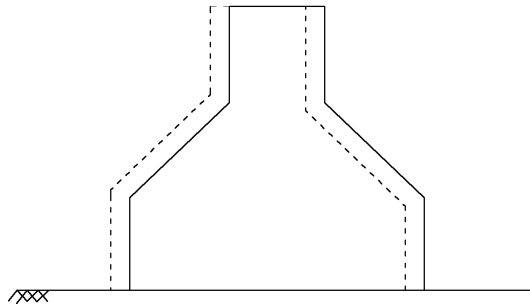


Figure 2.3: Pictorial representation of sliding failure mechanism

In addition to the above criterion, it should also be verified that the ratio of the horizontal and vertical load is less than 0.4.

2.2.3. SETTLEMENT CALCULATION

The SLS is more important than the ULS because this criterion defines the failure state of the structure even though the actual material failure is yet to be achieved. SLS is user-defined depending on the use of the structure. SLS criteria includes both total and differential settlements of the structure during its design life period. DNV [2] has clear guidance to assess these settlements by estimating:

- Immediate settlement, consolidation and creep (applicable for plastic soils),
- Cyclically induced settlement (caused by cyclic environmental loads),
- Lateral displacement and tilt (differential settlement)

It explains the calculation procedure for immediate and consolidation settlements caused by static loads, but it fails to explain the assessment procedure for the cyclically induced settlement although it is acknowledged. More details are given in the following subsections.

IMMEDIATE SETTLEMENTS

In DNV [2], the settlement calculation procedure is found to be based on either classical elastic method or Janbu's method based on the tangent modulus concept or even finite element techniques, that allows for realistic soil behaviour. Before doing so, the stress distribution with respect to depth before and after loading has to be calculated because the one-dimensional compression has a major influence in the settlement of the soil domain. One should always be aware that the non-linear stress-strain relationship of the soil can reduce the applicability of the elasticity theory. On the other hand, the results from elasticity theory match well with the settlement of many real-life structures. Thus, it can be recommended for the first order settlement calculation of the structure.

Stress distribution by Janbu's plasticity approach :

This approach takes into account the influence of the base plate stiffness on the stress distribution(2.5), which the elasticity theory fails to do. The stress distribution per unit length can be calculated by the equation:

$$\frac{\Delta\sigma'}{q_n} = 1 - 4h \int_0^z \frac{\tau_v}{q_n} d\zeta \tag{2.5}$$

Where the parameters: $h = \frac{H}{B}$; $\zeta = \frac{z}{H}$; $\tau_v = (\bar{\gamma}D + \gamma'z) K_p \tan \phi_m$;

ϕ_m must satisfy the bearing capacity formula: $q_n + \bar{\gamma}D = 0.5\gamma'BN_\gamma s_\gamma + \bar{\gamma}DN_q s_q$

s_γ & s_q can be calculated from above subsection 2.2.1

N_q & N_γ can be calculated from either above section or below figure 2.4

q_n is the uniformly distributed load [kN/m^2]

h is the dimensionless parameter [-]

B is the foundation breadth [m]

H is the foundation influence depth [m]

z is the depth of the layer [m]

$\bar{\gamma}, \gamma'$ are average unit weights above and below the foundation level, respectively [kN/m^3]

D is the foundation embedment depth [m]

K_p is the passive earth pressure co-efficient [-]

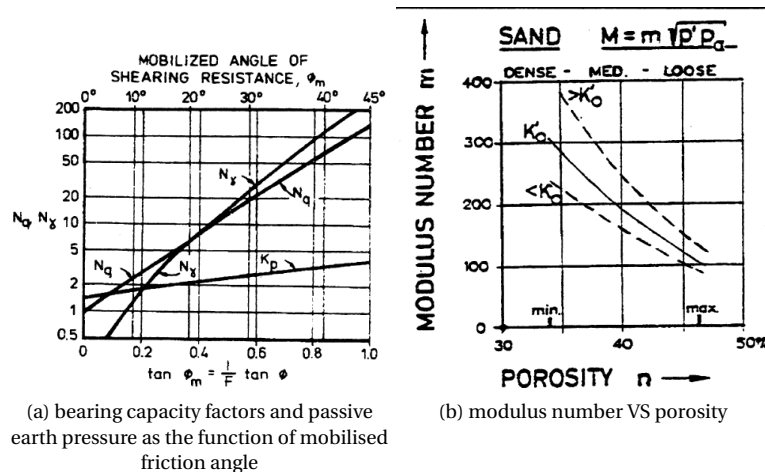


Figure 2.4: Graph from DNV [2] to find bearing capacity factors and modulus number

Settlement calculation by Janbu's tangent modulus concept:

The tangent modulus is a function of stress level, [18]

$$M = m\sigma_a \left(\frac{\sigma'}{\sigma_a} \right)^{1-a} \tag{2.6}$$

For sand: $a = 0.5$, stress dependency exponent. m , modulus number can be found from the chart 2.4

The total compression of the soil domain (until the influence zone) can be calculated by integrating the strain

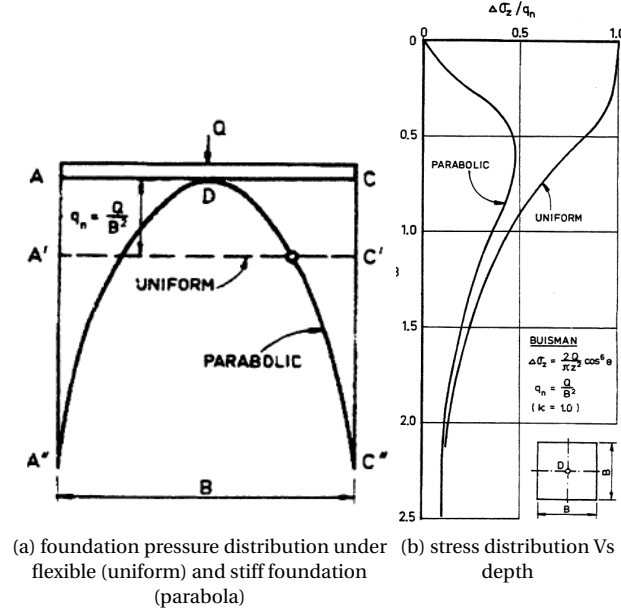


Figure 2.5: The influence of the base plate stiffness on stress distribution with respect to depth

over the influence depth.

$$\delta = \int_0^H \varepsilon_z dz; \quad (2.7)$$

From the well known Hook's law:

$$\varepsilon = \int_{\sigma'_{vo}}^{\sigma'_{vo}} \frac{d\sigma'}{M}; \quad \varepsilon = \frac{2}{m} \left[\sqrt{\frac{\sigma'_{vo} + \Delta\sigma}{\sigma_a}} - \sqrt{\frac{\sigma'_{vo}}{\sigma_a}} \right]$$

where, σ_a is the reference stress (100kPa) [kPa]

σ' is the effective stress in the layer [kPa]

ε is the strain in Z direction [-]

δ is the settlement in Z direction [m]

Eventually, the area of the plot between ε & depth for each layer can be calculated, which is equal to the settlement [2].

2.2.4. DYNAMIC RESPONSE

It is well known that the loading and the structural responses are both site and purpose specific. Principally the support structure of the offshore wind turbine is subjected to large moment loading at the seabed because of the horizontal load created by the wind and waves. Therefore, the foundation should be stiffer, which is able to transfer the moment. Moreover, it should also be verified that loading frequencies don't coincide with the natural frequency of the structure because it leads to the resonance condition that can destabilise the structure. In general, two excitation frequencies called rotor and blade passing frequency (1P and 3P respectively) are considered for the verification. The excitation ranges and the realistic spectrum of hydrodynamic excitation for typical turbines are shown in the figure 2.6. The aerodynamic spectrum is not presented as it is less than the wave spectrum.

In the figure 2.6, the frequency range in which the current design of support structure for offshore wind turbine lie is evidenced (soft-stiff). The wind energy sector refers the range as "soft-stiff" structure, as the natural frequency of the structure is between 1P and 3P. However, it is also possible to design the support structure with a natural frequency below the first excitation frequency 1P, which is called "soft-soft" structure, or with a natural frequency above the blade passing frequency 3P, for a 3-bladed wind turbine, which is called "stiff-stiff" structure. Eventually, the choice of frequency range sets a requirement for the stiffness of the foundation.

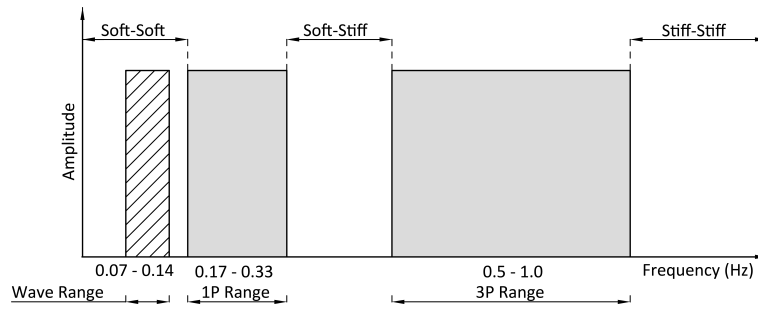


Figure 2.6: Excitation frequency range for offshore wind turbine (Prendergast et al, 2015 [3])

The foundation stiffness should be determined based on the strength and stiffness of the soil as well as on the structural foundation elements. In numerical analysis, springs are often used to represent the soil. The non-linear behaviour of soil sets the prerequisite to model springs at different support points with various modes of action such as vertical, horizontal, torsional and rocking. Since the foundation is used to support an offshore wind turbine, we are interested in rocking (rotational) stiffness as the moment loading is predominant. The rocking stiffness represents the ratio between the overturning moment (M) and the rotation angle (θ) in rocking. In order to evaluate the different stiffness of various springs, shear modulus (G) of the soil is used in general [13]. Once the stiffness is known, the frequency can be found by the following formula.

$$f = \frac{1}{2\pi} \sqrt{\frac{k}{m}} \quad (2.8)$$

where, k is the stiffness and m is the mass of the structure.

2.2.5. SOIL STRENGTH DEGRADATION

The above-explained sub-sections clearly exhibit the methods to overcome common geotechnical issues encountered by the foundation according to DNV, an international standard. An important issue called degradation of soil strength in response to cyclic loading is not dealt so far.

PORE PRESSURE ACCUMULATION

The cyclic behaviour of the soil should be analysed considering the fact that shearing would cause the pore pressure to either build or dissipate depending on the state of the soil. Hence, every possible pore pressure contribution should be taken into account for the analysis. The possible pore pressure contributions are

- Initial in-situ pore pressure,
- pore pressure during installation,
- pore pressure due to cyclic loading, and
- pore pressure due to transient loading.

The pore pressure contour diagrams derived from the undrained cyclic test can be used to derive the pore pressure build-up [19]. It should also be noted that the contour diagrams must be site specific and for various stress levels. Pore pressure response between low and moderate stress levels is recommended to be derived from,

$$R_u = \Delta\sigma_d \frac{dN}{du} \quad (2.9)$$

where,

R_u is the cumulative pore pressure resistance $R_u = r_u * N$ [kN/m^2]

N is the number of cycles at stress level $\Delta\sigma_d$ [-]

r_u is determined from the laboratory tests [kN/m^2]

$\Delta\sigma_d$ is the deviatoric stress [kN/m^2]

The pore pressure response due to transient undrained loading can be defined by,

$$\Delta u = \Delta\sigma_m - D\Delta\sigma_d \quad (2.10)$$

where,

Δu is the change in pore pressure resistance [kN/m^2]

$\Delta\sigma_m$ is the change in mean total stress $\frac{1}{3}(\Delta\sigma_1 + \Delta\sigma_2 + \Delta\sigma_3)$ [kN/m^2]

$\sigma_1, \sigma_2, \sigma_3$ are major, intermediate and minor principal stresses, respectively [kN/m^2]

D is dilatancy parameter [-]

$\Delta\sigma_d$ is the change in deviatoric stress [kN/m^2]

Even though the international standard, DNV, highlights the procedure to evaluate the cyclic degradation of shear strength due to pore pressure generation, it requires extensive laboratory testing for each individual site which is of less interest for industries because of the involved cost and time. Moreover, It also fails to define parameters like r_u and the procedure to obtain it.

STIFFNESS DEGRADATION

It is worth noting that the change in pore pressure results in a change in effective stress which eventually causes the change in stiffness. As an international standard, DNV does recommend to use the one of the following undrained shear strengths in foundation design. They are,

- static shear strength reduced for the effect of cyclic loading,
- cyclic shear strength, defined as the sum of static and cyclic stress that caused failure for a given number of cycles.

They also emphasize to use cyclic shear strength in the cases where cyclic effects are significant but they did not elaborate the method to assess the stiffness degradation similar to API.

Lupea (2013) [7] used a stiffness reduction method as recommended in geotechnical earthquake engineering in her dissertation of proposing a simplified alternative approach to assess the long-term response of suction caisson under vertical cyclic loading. The equation adopted was,

$$R_u = 1 - \frac{\tan\phi'_{red}}{\tan\phi'_{initial}} \quad (2.11)$$

where,

R_u is the ratio of excess pore water pressure to effective vertical stress $R_u = \frac{p_{excess}}{\sigma'_v}$ [-]

ϕ'_{red} is the reduced friction angle of sand [$^\circ$]

$\phi'_{initial}$ is the initial friction angle of sand [$^\circ$]

There are also several other models including both empirical and constitutive similar to the one used by Lupea and they are explained in the following sections.

STRAIN ACCUMULATION

The change in pore pressure, apart from shear strength evolution, also leads to the change in strain or displacement. Since the frequency of loading is larger, the pore pressure build-up affects the effective stress in the soil domain. Thus, the accumulation of strain can be readily visible. Witchman (2005) [20] witnessed no convergence in the accumulation of strain even in the higher cycle numbers in his model. His model is an advanced model that analyses strength in every element.

DNV, as an international standard, emphasizes the importance of settlement calculation as explained in the above sub-sections. They have also mentioned about the settlement during cyclic loading. It includes settlement caused by undrained shear deformations, and by the consolidation of pore pressures generated by the cyclic loading. They recommend the usage of analytical soil models capable of assessing the average shear stress and the cyclic shear history in all soil elements. Unfortunately, no further information or guidance is given. However, several research proved the components which result in the settlement (Andersen & Hoeg 1992, Yildirim & Ersan 2006)[21][22]. These research concluded that the reduction in shear modulus because of the build-up of negative excess pore pressure cause the settlement during cyclic loading. Further, the reduction in volume resulting from pore pressure dissipation induce the settlement after cyclic loading (during the calm period).

In this section, an overview of the design procedure for the GBF is given in accordance with an international standard DNV. The foundation must be designed with respect to bearing capacity, stability against sliding, settlements, dynamic response, and cyclic response. Each geotechnical issue is explained with the guidance of DNV and other literature. Besides, it also emphasizes the complexity and the lack of concentration in cyclic response. Thus, it can be concluded that a step towards understanding the cyclic response can further help in the optimisation of the foundation making it cost-efficient.

2.3. RESPONSE OF THE FOUNDATION TO CYCLIC LOADING

The response of the foundation to cyclic loading, as defined in DNV, clearly requires further investigation that enables a clear and optimised procedure for the design of GBS foundation. Eventually, it helps to improve the economic feasibility of future offshore wind farms. There were several research in the past that contribute to the design procedure for the foundation founded on both clay and sand domain [23][9][24]. Sandy soil is the area of interest because of their predominant presence in the North sea. Thus, naturally it leads to concentrate on the research focused on the sand. Several academic research groups such as University of Western Australia, Oxford University, Aalborg University, and Karlsruhe Institute of Technology dominated the research on sand both experimentally and numerically. [9][25][17][20].

Researchers at Oxford University are well established for their contribution to the design industry through their work on physical modelling. The facility to model using three degree-of-freedom loading device helped to explore the response of the foundations subjected to combined loading [25]. They aided in the development of the failure envelope for combined loading and so generalise the bearing capacity calculation depending on the combined loading rather than vertical loading. The plastic response of the footing is analysed, in detail, in accordance with the hardening law and flow rule appropriate for a plasticity model [26]. Byrne (2004) [25] showed that the extreme events cause the yield surface to extend according to the plasticity theory. Hence the response of the foundation under the general working condition is inside the yield surface and thus elastic deformation is evident. Eventually, the elastic response in long-term cyclic vertical loading was proved by Lupea (2013) [7] in her master thesis.

Similarly, the University of Western Australia is well established for their work on numerical modelling. In the event of providing additional support to the research [26][25], Gourvenec (2004)[9] proved that the classical bearing capacity formulas such as Brinchen Hansen, Terzahi, and Vesic underestimates the ultimate limit states for relevant offshore foundations, whereas the failure envelope shows the exact behaviour of offshore foundations without any discrepancy under general loading conditions. Therefore, the best possible way to represent the capacity of the foundation will be through the failure envelope for the particular foundation under combined loading. The complexity in the interaction between vertical, horizontal and moment loading was evident from many research and so it is not simple to extrapolate the failure envelope for the specific case from the benchmark solutions provided in the past. Hence, several researchers Bransby & Randolph(1998)[27]; Taiebat & Carter (2000) [23]proposed different expressions that aided in developing the failure envelope. But they were proved to be limited for particular soil conditions and foundation dimensions by Gourvenec (2007) [9]. In the same paper, she proposed an alternative approach that predicts the failure envelope with more accuracy.

In this context, the importance of the combined loading response on the offshore foundations and the discrepancy in the current design guidelines API and DNV were brought into the light. The combined horizontal and moment loads resulting from environmental conditions (wind and waves) acts cyclically on the structure. Byrne et al (2002) [24] realised the importance of cyclic loading effects on the foundation and took the significant challenge of modelling cyclic loads accurately. They ended up with a theoretical model of continuous hyper plasticity. The model is also proved to predict the cyclic response of suction caisson foundation, with the help of experimental set up mentioned above. Alongside, they proved the strong correlation between monotonic and cyclic loading based on the masing's rules by comparing the vertical load and stiffness.

EFFECT OF CYCLIC LOADING ON PORE PRESSURE, STIFFNESS AND SETTLEMENT

The importance of offshore foundation response on cyclic loading was realised in early 2000, which resulted in several research and continued in the current century as well [15][25][21]. Current generation researchers have concentrated the same in different foundations such as monopiles [17] and suction caisson [28][7]. As explained earlier in this chapter, the gravity based foundation response is yet to be explored.

Predominantly, the response of the foundation is manipulated by the drainage type of the soil domain, on which it is installed. This is because the drained behaviour allows no pore pressure build-up whereas undrained behaviour does and lead to changes in effective stress (the soil response is explained in the above section

2.2.5). The drainage type depends on several factors such as permeability, drainage length, soil modulus, porosity, and amplitude and the frequency of the applied load (Zienkiewicz et al (1980)) [29].

Sand being partially drained in practical applications has more tendency to increase pore pressure build-up, which in turn influence the foundation capacity. Also, pore pressure build-up can be expected during the cyclic loading as the frequency would be between 0.07 and 0.14 HZ in general (Prendergast et al, 2015) [3]. Liquefaction can occur in loose sands, resulting in either loss of stiffness or most of its strength. Apparently, It is evident from Ekofisk I platform where dense sand contracts under cyclic loading which pave way for excess pore pressure build-up even though they tend to dilate under monotonic shearing [8]. There are several constitutive models which are able to assess the pore pressure build-up such as Hypoplastic sand model, UBC sand model, Hybrid model by C.Pasten, etc. [30] [31] [32]. Each model is clearly described in the following sections.

RESPONSE OF MONOPILES ON SAND TO LONG-TERM CYCLIC LOADING

The design of piles is based on API whereas DNV concentrates more on GBS foundation as explained above. It is worth noting that the design guidelines in API were also formulated from offshore oil & gas sector. The soil-structure interaction in laterally loaded piles is based on p-y curves that evolved from oil & gas sector and empirical formulas. The load characteristics of wind turbines (predominant moment loading) is significantly different from the support structure in oil and gas industry. Hence the reliability of p-y curves for pile design in offshore wind energy sector is a great question. Le Blanc (2009) [17] proved that the guidance to design pile foundations subjected to strong cyclic loading is limited and helped to improve it. Similar to Byrne et al (2002) [24] his research also proved that the structural stability is dominated by serviceability limit states over a span of 25 years than ultimate limit states. Moreover, it is evident from his results of physical modelling that the long-term cyclic lateral loading in foundation induces the accumulation of plastic deformation in the soil domain, which in turn changes the stiffness of the surrounding soil. In particular, the dependency of accumulated rotation on relative density and load characteristics was proven. Furthermore, the pile stiffness is observed to increase with respect to number of cycles as a result of plastic deformation. This is in contrast with the current methodology [16]. The increase in stiffness increases the capacity of the foundation which raises the doubt of response in GBE.

It is also well established that the foundation response to axial cyclic loading leads to accumulation in displacement and decrease in stiffness Jardine et al (2012) [33]. Additionally, they have also reviewed research that were concentrated on response to cyclic lateral loading. From their conclusion, it is clear that the research Peralta (2010) [34] on rigid foundations goes in line with the results of Le Blanc (2009) [17] as well.

RESPONSE OF SUCTION CAISSON ON SAND TO LONG-TERM CYCLIC LOADING

Lupea (2013) [7] investigated computationally the response of suction caisson foundation to vertical cyclic loading with the help of hybrid model. Her concentration was in pore pressure that reduces the effective stress and so the shear strength. Her dissertation proved the overestimation in pore pressure build-up, in particular from her model. Eventually, she concluded proving that the foundation response is in the elastic region almost throughout their design life which is approximately 20-25 years.

Furthermore, model caisson was tested in several 1-g tests by B.Zhu et al (2013) [28] on an in-house experimental set-up that was capable of modelling under three degree-of-freedom loading device [25]. They concentrated on fatigue limit state (FLS), in particular with accumulated rotation and stiffness. It was found that the magnitude of accumulated rotation decrease with number of cycles. Despite the change in the accumulated rotation the change in stiffness was found to be insignificant. This is different from the behaviour of monopiles as reported by Le Blanc (2009) [17]. Therefore, the change in dynamic characteristics remains unaltered. They have also suggested a theoretical model that represents the accumulated rotation non-dimensionally as a function of number of cycles. It is,

$$\frac{\Delta\theta(N)}{\theta_s} = T_b(\zeta_b) * T_c(\zeta_c) * N^\alpha \quad (2.12)$$

where,

$\Delta\theta(n)$ is the change in accumulated rotation during cyclic loading [-]

θ_s is the accumulated rotation during monotonic loading [-]

ζ_b, ζ_c are the load characteristics [-]

T_b, T_c are dimensionless parameters function of the load characteristics [-]

α is the exponent [-]

It is evident that the model is in the same form as the one expressed by Le Blanc .

RESPONSE OF GBS FOUNDATIONS ON SAND TO LATERAL CYCLIC LOADING

Vanwijngaarden (2017)[35] in his thesis assessed the liquefaction potential of the soil under GBF. He investigated the development of excess pore pressure along with the cyclic shear stress profile in the soil domain. The conclusion clearly depicts that the pore pressure build-up is more detrimental for the short-span storm with high frequency rather than long-span storm with high amplitude. Moreover, no liquefaction is evidenced in the case of sand with a relative density of 60%, but one can conclude that the build-up in pore pressure can reduce the stiffness of the soil. Eventually, the reduction in stiffness can change the capacity of the foundation which should be verified in order to make the design safe.

In this section, the effect of cyclic loading on foundation response is discussed in detail. The predominant dependency of drainage type on the pore pressure behaviour is explained. One can conclude from the above section that the failure envelope estimates the behaviour of the foundation without any discrepancy which the classical bearing capacity equations failed to do. In the end, the stiffness increase in the case of monopiles in response to long-term cyclic loading and insignificant change in the case of suction caisson increases the doubt in the response of the GBF.

2.4. BASE CASE OF GRAVITY BASED FOUNDATION

A commercially available 5MW wind turbine is chosen for this analysis and their anticipated loads are calculated in following sub-sections. A base case foundation for it is designed which is used to find the effect of pore pressure build-up on the capacity of the GBF. The loads considered for the preliminary design are presented in the table 2.1. The base case design is in accordance with the international standard, DNV [13] as explained in the previous section.

Type	Load	Units
Total dead load	153.5	<i>MN</i>
Horizontal load	9.537	<i>MN</i>
Moment	451.910	<i>MN – m</i>

Table 2.1: Loads without considering the design factors used in the preliminary design

2.4.1. LOADS ON THE OFFSHORE WIND TURBINE

PERMANENT LOADS

The dead load from 5MW wind turbine with the hub height of 90 m+MSL is calculated from the technical report by Jonkman et al (2009) [36].

Type	Load	Units
Dead load from structure (turbine)	6.84	<i>MN</i>
Dead load from concrete (foundation)	73.66	<i>MN</i>
Dead load from ballast	72.95	<i>MN</i>

Table 2.2: The permanent load of a 5 MW wind turbine including the foundation

WIND LOADS

For this dissertation, the aerodynamic wind loads are calculated in accordance with the research work by Vanwijngaarden (2017)[35]. Assuming the maximum wind speed of 25 m/s, the wind load and the corresponding moment is calculated. The detailed procedure of the calculation is presented in the Appendix A. The resulting load and the moment at the sea bed is given in the table 2.3

Parameter	Value	Units
<i>Wind load</i>		
Wind speed (assumed)	25	<i>m/s</i>
Horizontal load	1.2	<i>MN</i>
Height of the structure	130	<i>m</i>
Moment at the sea bed	161.6	<i>MN – m</i>
<i>Wave load</i>		
Water depth (d)	35	<i>m</i>
Significant wave height (H_s)	8.5	<i>m</i>
Significant wave period (T_s)	13	<i>s</i>

Table 2.3: Parameters used for the load calculation (both wind and wave)

WAVE LOADS

The hydrodynamic wave loads are calculated based on the semi-empirical relation called Morison equation [10]. It calculates the wave loads by combining the two forces namely; the inertia and drag force. The original version of it is valid only for the slender structures. In order to extend the validity for the structure with a large diameter, some modifications were made [37]. Even then, the equation is limited to a first approximation. The assumptions used for the calculation of the wave load is given in the table 2.3.

The load distribution in the foundation as a function of depth is shown in the figure 2.7. A detailed explanation of the wave load calculation is given in Appendix A.

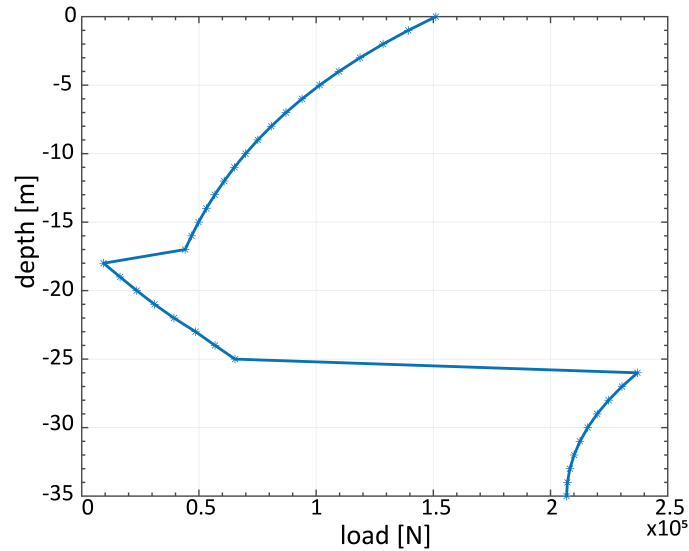


Figure 2.7: Maximum horizontal hydrodynamic load resulting in the foundation

2.4.2. GRAVITY BASED FOUNDATION DIMENSIONS

The designed base case foundation is shown in the figure 2.8. It should be noted that the design doesn't consider the cyclic loads as it is just the base case but the author recommends to consider the cyclic response for the final design. Therefore, one can conclude that the design used in this research satisfies the geotechnical requirements such as the bearing capacity, consolidation settlement and differential settlement.

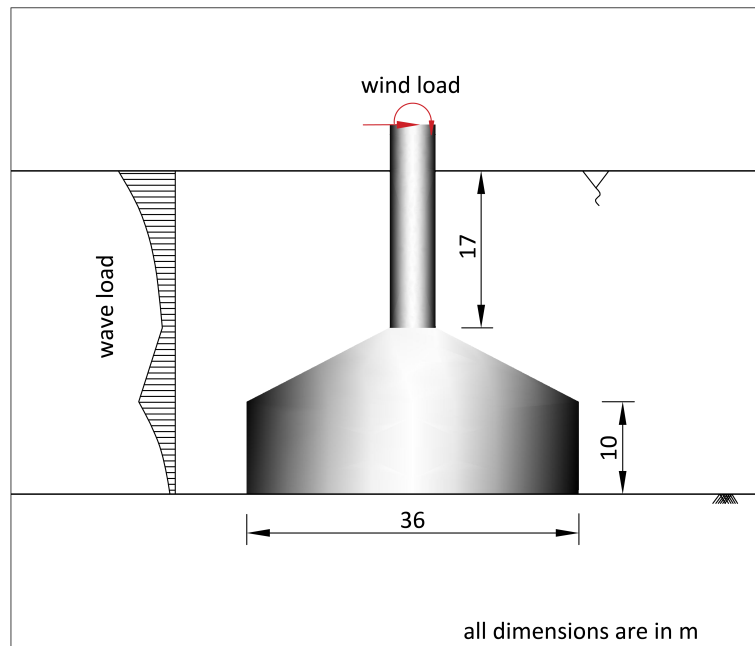


Figure 2.8: Geometry of the gravity based foundation used in this thesis

The foundation in the figure 2.8 shows the dimensions along with the chosen shape as well.

2.4.3. FAILURE ENVELOPE UNDER COMBINED LOADING

Since it is concluded that the classical bearing capacity formulae underestimate the capacity [9], a failure envelope under combined loading is developed and compared with the design made. The failure envelope is developed for the particular vertical load of 153.5 MN and it is shown in the figure 2.9. Both the moment and horizontal load is divided by the diameter of the foundation (D)

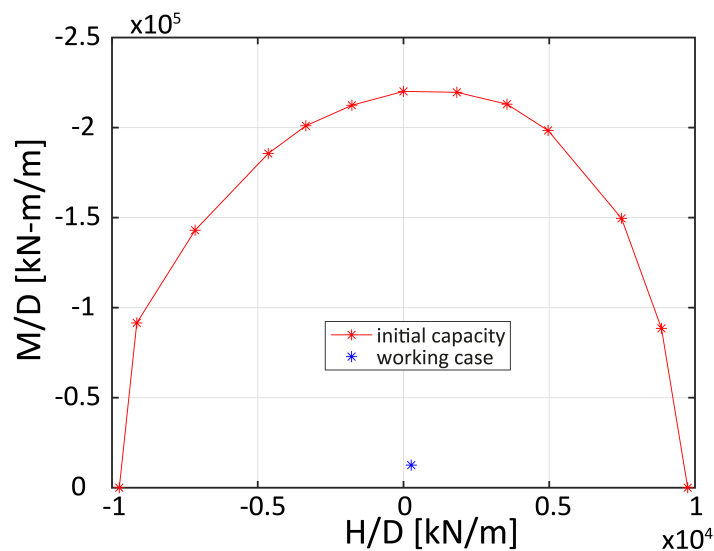


Figure 2.9: Failure envelope of the foundation under combined loading in static condition

It is evident from the figure that the base case foundation is conservative (as the working load is away from the boundary of the failure envelope). Therefore, GBF shown in the figure 2.8 can be used in this analysis without any doubts.

The development of failure envelope involves analysis with different load combinations of horizontal and moment load (as they are the dominant and varying loads in our case). The resulting pure horizontal and

moment capacities under working vertical load is shown in the figure 2.10.

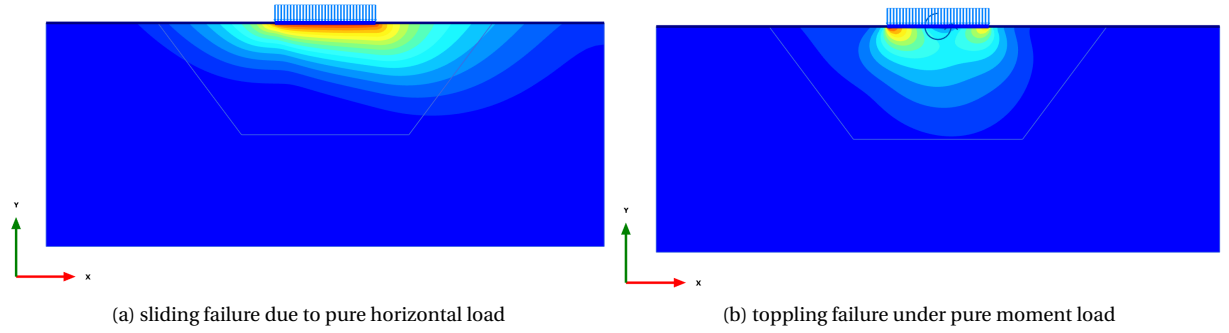


Figure 2.10: Failure surface generated under working vertical load

The resulting failure surface clearly explains that the foundation tends to slide under pure horizontal load and topple under pure moment load. They also help in defining the mesh refinement area as explained in chapter 3 [3.4].

2.5. ADVANCED CONSTITUTIVE MODELS

In order to achieve more realistic behaviour, finite element modelling is preferred rather than theoretical models as represented in DNV. Exploring the disadvantage of respective models, several constitutive models were derived that takes into account the cyclic behaviour of soil and their resulting response such as pore pressure accumulation and strain accumulation. They are UBC sand model, Hypoplastic sand model, Hyperplastic model, Hybrid model and others. [31] [30] [26] [20] [32] [38]

2.5.1. ELASTOPLASTICITY MODELS

UBC SAND MODEL

UBC sand model is one of the advanced soil models developed at the University of British Columbia with the aim of predicting the liquefaction in sandy soils. It incorporates two yield surfaces that helps in calculating the accumulation in both strain and pore pressure due to cyclic loading. [31]

The UBC sand model is based on the well established Mohr-coulomb yield functions. The full set of yield functions both in compression and tension is given below:

$$\begin{aligned}
 f_{1a} &= \frac{1}{2}(\sigma'_3 - \sigma'_2) + \frac{1}{2}(\sigma'_3 + \sigma'_2) \sin \phi' - c' \cos \phi' \\
 f_{1b} &= \frac{1}{2}(\sigma'_2 - \sigma'_3) + \frac{1}{2}(\sigma'_2 + \sigma'_3) \sin \phi' - c' \cos \phi' \\
 f_{2a} &= \frac{1}{2}(\sigma'_1 - \sigma'_3) + \frac{1}{2}(\sigma'_1 + \sigma'_3) \sin \phi' - c' \cos \phi' \\
 f_{2b} &= \frac{1}{2}(\sigma'_3 - \sigma'_1) + \frac{1}{2}(\sigma'_3 + \sigma'_1) \sin \phi' - c' \cos \phi' \\
 f_{3a} &= \frac{1}{2}(\sigma'_2 - \sigma'_1) + \frac{1}{2}(\sigma'_2 + \sigma'_1) \sin \phi' - c' \cos \phi' \\
 f_{3b} &= \frac{1}{2}(\sigma'_1 - \sigma'_2) + \frac{1}{2}(\sigma'_1 + \sigma'_2) \sin \phi' - c' \cos \phi'
 \end{aligned} \tag{2.13}$$

where,

$\sigma'_1, \sigma'_2, \sigma'_3$ are the major, intermediate and minor principle effective stresses, respectively [kN/m^2]

ϕ' is the effective friction angle [$^\circ$]

c' is the effective cohesion [kN/m^2]

The above formulae help in the construction of yield surface 2.11 within which the elastic behaviour can be evidenced when the stress state is inside. Stress state, on reaching the yield surface initiates the plasticity

through hardening rule. The elastic behaviour is governed by a non-linear rule which is controlled by two stiffness parameters as follows,

$$k = k_B^e P_A \left(\frac{p}{p_{ref}} \right)^{m_e}; G = k_G^e P_A \left(\frac{p}{p_{ref}} \right)^{n_e} \quad (2.14)$$

where,

p' is the mean principle effective stress [kN/m^2]

p_A is the atmospheric pressure (100kPa) [kPa]

K_B^e is the elastic bulk modulus [kN/m^2]

K_G^e is the elastic shear modulus [kN/m^2]

m_e is the elastic bulk modulus index [-]

n_e is the elastic shear modulus index [-]

The plasticity behaviour is governed by the shear hardening rule similar to hardening soil model,

$$d\gamma^p = \frac{p'}{G_i^p} \left[1 - R_f \left(\frac{\sin \phi_m}{\sin \phi_p} \right) \right]^{-2} \quad (2.15)$$

where,

G_i^p is the plastic shear modulus at onset of shear mobilisation [kN/m^2]

ϕ_m is the mobilised friction angle [$^\circ$]

ϕ_p is the peak friction angle [$^\circ$]

R_f is the failure ratio [-]

Shear hardening is a type of hardening in which plastic strain develops by mobilising the shear strength of the soil. The direction of plastic strain is defined by plastic potential function as the flow rule is assumed to be non-associated. The plastic potential function is as follows:

$$g = q - \alpha (p' + c \cot \phi_p) \quad (2.16)$$

where,

q is the deviatoric stress [kN/m^2]

p' is the mean effective stress [kN/m^2]

α is the parameter that helps in finding the steepness of the cap and can be found from K_o^{nc} [-]

c is the cohesion [kN/m^2]

ϕ_p is the peak friction angle [$^\circ$]

A non-associated flow rule is defined, which is based on the following three observations:

- Unique stress ratio defined by ϕ_{cv} where neither contraction nor dilation occurs,
- Stress ratio below ϕ_{cv} represents the contraction and above the dilation behaviour,
- The amount depends on the ratio between current stress ratio and stress ratio at ϕ_{cv}

the relationship is

$$\begin{aligned} d\epsilon_v^p &= \sin \psi_m d\gamma^p \\ \sin \psi_m &= \sin \phi_m - \sin \phi_{cv} \end{aligned} \quad (2.17)$$

where,

$d\epsilon_v^p$ is the plastic volumetric shear increment [-]

$d\gamma_v^p$ is the plastic shear increment [-]

ϕ_{cv} is the friction angle at critical state [$^\circ$]

As explained above, this model incorporates two different yield surfaces (fig:2.11) where one defines the failure and the other defines the unloading and reloading based on the mobilised friction angle. This paves way for the smooth transition towards liquefaction. The plasticity shear modulus k_G^p is formulated separately for the secondary loading based on the number of cycles in the loading progress.

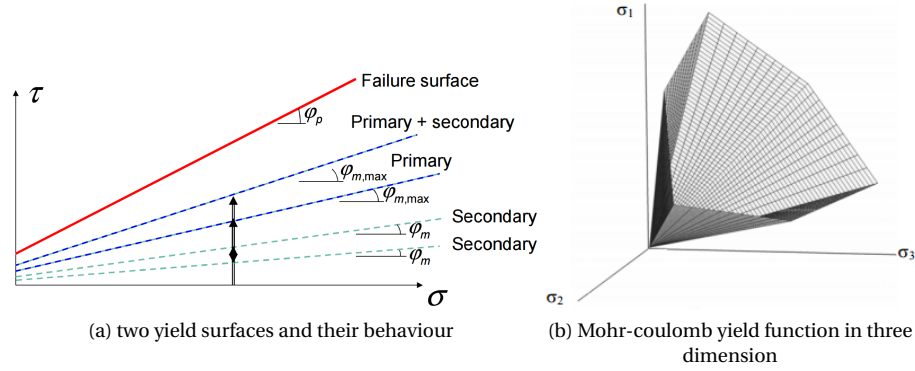


Figure 2.11: Shape of different yield surfaces [4]

$$k_G^p = k_G^p * \left(4 + \frac{n_{rev}}{2}\right) * hard * fac_{hard} \quad (2.18)$$

where,

k_G^p is the plasticity shear modulus [kN/m^2]

n_{rev} is the number of shear stress reversals from loading to unloading or vice versa [-]

$hard$ is the factor correcting densification rule for loose soils [-]

fac_{hard} is the multiplier used to adjust the densification rule [-]

Despite having the capability of including accumulation of strain and pore pressure, the response is not realistic particularly for our case (i.e., cyclic loading in long-term). Moreover, the compaction hardening is not incorporated which may allow the stress state to move beyond the failure envelope.

2.5.2. HYPOPLASTICITY MODELS

These models are different from the above discussed elastoplastic models. This model is based on the hypoplasticity that describes the realistic behaviour of the soil (i.e., non-linearity and in-elastic components). Hypoplasticity is defined by Fellin (2002)[39] as a constitutive law of rate type and it is the relation which associates the strain rate to the stress rate.

As in elastoplastic models, the strain is not differentiated into elastic and plastic components. Instead, the rate equation is used to formulate the inelastic behaviour (in other words inelastic behaviour of the hypoplastic constitutive law is modelled by using the modulus of strain rate). Moreover, it uses neither yield surface nor plastic potential function. Even without using them, they predict all the important soil behaviour such as critical state, stress dependency of stiffness, etc. using the rate type equations.

HYPOPLASTIC SAND MODEL

The general version of the hypoplastic sand model in the tensor formulation is presented in the equation 2.19. The general version by Gudehus (1996)[30] is the modified form of the original law. The equation includes the influence of density (pycnotrophy) and stress level (barotrophy).

$$\dot{T} = f_e f_b [L(\hat{T}, D) + f_d N(\hat{T}) \|D\|] \quad (2.19)$$

where,

\hat{T} is the objective stress rate tensor

D is the deformation rate tensor

L is the stress-dependent tensor related to linear part

N is the stress-dependent tensor related to non-linear part

$\hat{T} = T(t)$ is the granulate stress ratio tensor

f_e is the pycnotrophy factor (density dependency)

f_b is the barotrophy factor (stress dependency)

f_d is the pycnotrophy factor related to material state

The original law was formulated by Von wolffersdorff (1996)[40]. He incorporated the Matsuoka-Nakai criterion as the failure criterion instead of Mohr-coulomb failure criterion. The below figure 2.12 clearly shows the advantages of matsuoka-nakai than Mohr-coulomb failure criterion[5]. Considering the advantages, the same failure criterion was used by Gudehus (1996)[30] in the general version of the hypoplastic model.

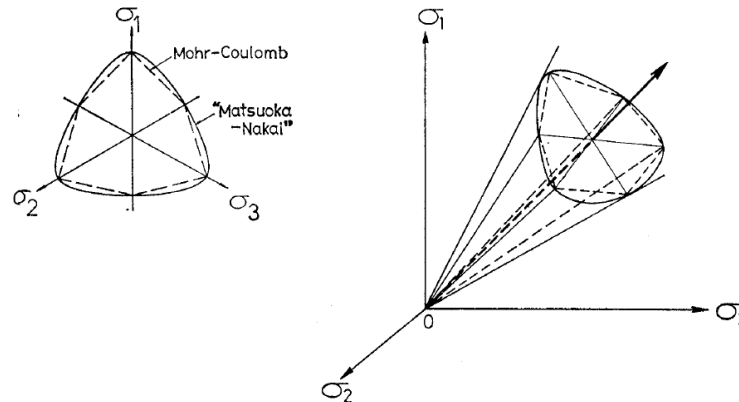


Figure 2.12: Failure criterion comparison between Mohr-coulomb and matsuoka-nakai criteria (Matsuoka & Nakai (1985))[5]

The parameters of the hypoplastic-sand model is presented in table 2.4:

Symbol	Description
ϕ_c	Critical state friction angle
h_s	Granular hardness
n	Exponent of compression law
e_{do}	Void ratio at maximum density for $p = 0$
e_{co}	Void ratio at critical state for $p = 0$
e_{io}	Void ratio at minimum density for $p = 0$
α, β	Pycnotrophy exponents controlling the dependency of peak friction angle and soil stiffness on relative density

Table 2.4: Parameters of hypoplastic sand model

The model calibration procedure:

Herle & Gudehus (1999)[6] explained the procedure to obtain the hypoplastic sand model parameters from the result of laboratory experiments.

- Critical state friction angle (ϕ_c): It is a friction angle at the critical state where there is no volumetric deformation. The critical state can be achieved when both the stress state and the volumetric deformation rate vanish during monotonic shearing. Apparently, it can be obtained from the angle of repose as well[6]. They have shown that the critical state friction angle and the angle of repose match in almost all sands. The below figure 2.13 shows the measurement of the angle of repose and the comparison of the critical state friction angle & the angle of repose by authors.

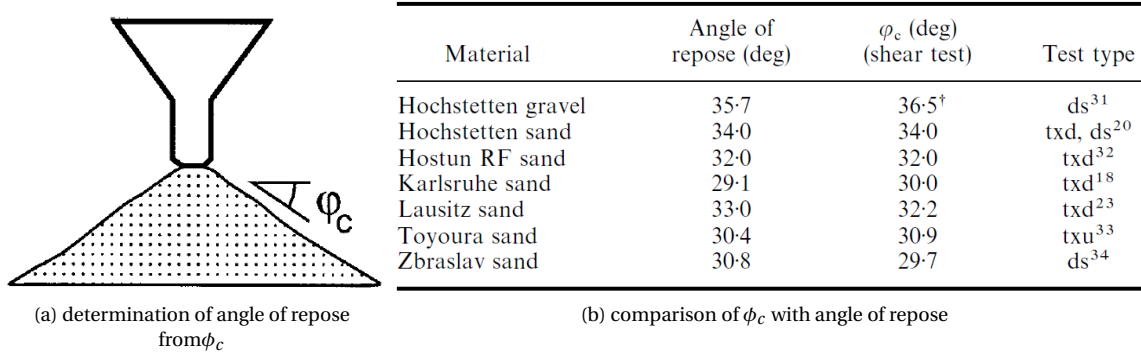


Figure 2.13: Measurement of angle of repose [6]

- Granulate hardness (h_s) and exponent (n): The granulate hardness h_s with the units of stress and the dimensionless parameter, exponent n influences the shape of the compression curves. The current step void ratio can be found from the void ratio at zero pressure using these parameters by the following equation:

$$e_p = e_{p0} \exp \left[- \left(\frac{3p_s}{h_s} \right)^n \right]$$

$$h_s = 3p_s \left(\frac{ne_p}{C_c} \right)^{1/n} ; n = \frac{\ln(e_{p1}C_{c2}/e_{p2}C_{c1})}{\ln(p_{s2}/p_{s1})}$$

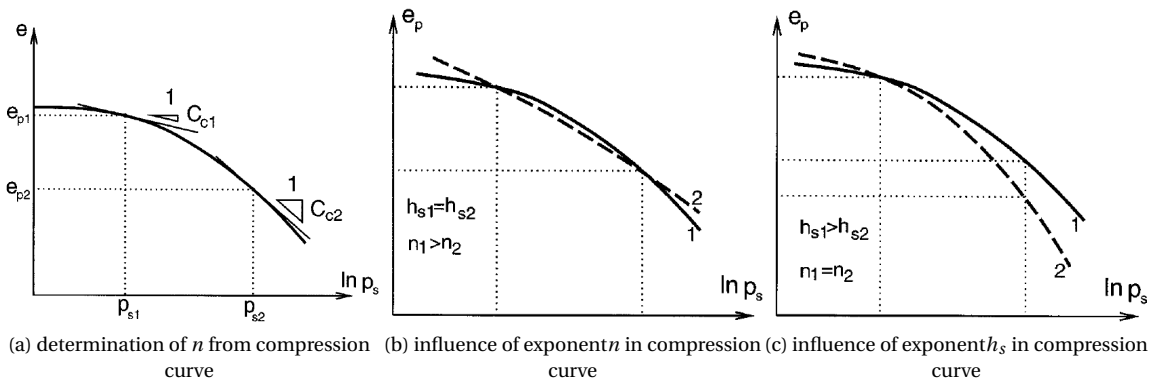
where,

p_s is the average limit value of p [kPa]

e_p is the average limit value of e [-]

C_c is the secant compression index [-]

The exponent (n) allows the non-proportional increase of the incremental stiffness with increasing p_s whereas h_s controls the slope of the compression curves. The influence of n and h_s on compression curves and the determination of n are graphically represented in the following figure 2.14.

Figure 2.14: Determination of n and Compression curve showing the influence of n & h_s on them [6]

- Minimum and maximum void ratio: The minimum and maximum void ratio of a soil are more common parameters which can be found from the index tests as prescribed in the international standards. But one should be aware the parameters are found at zero pressure.
- Critical state void ratio: The critical state void ratio should be the function of the pressure as the limiting void ratio should reduce when the pressure p_s increases. A general picture of limiting void ratio in

relation with pressure is shown in the below figure 2.15. Lupea (2013)[7] suggested the simplest way that, the initial void ratio of the loose sand in oedometer test can be considered as an appropriate estimate of e_{co} . Therefore, e_c can be found from:

$$e_c = e_{co} \exp \left[- \left(\frac{3p_s}{h_s} \right)^n \right]$$

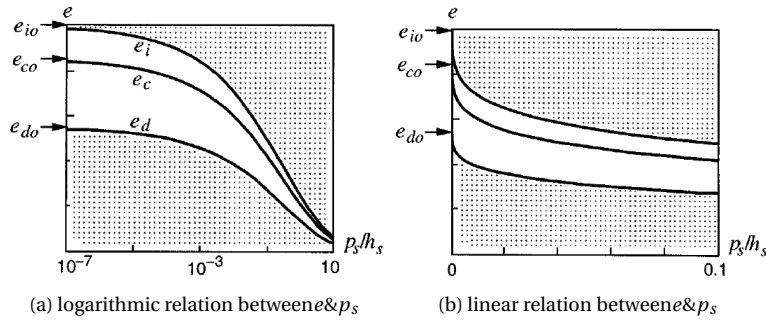


Figure 2.15: Relation between void ratio e and pressure p_s [6]

- Parameter α & β : Lupea (2013)[7], suggested a simple way to calibrate these parameters from triaxial tests. α controls the relation between relative void ratio and peak friction angle and β controls the size of the failure envelope.

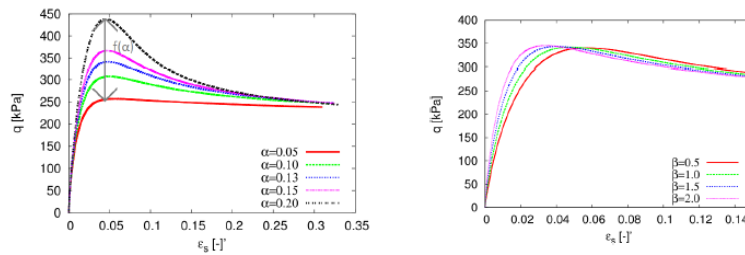


Figure 2.16: Determination of parameter α & β [7]

As presented in the figure 2.16, the best way to calibrate these parameters is by fitting the curve of shear strain in a triaxial test.

INTERGRANULAR STRAIN CONCEPT

Niemunins & Herele [41] attempted to model the small strain stiffness effects in hypoplasticity which resulted in the intergranular strain concept. Five parameters that capture the small strain stiffness effect are incorporated in the hypoplastic sand model and these parameters are,

- m_R is a parameter that controls the initial shear modulus upon 180° strain path and initial loading. They can be calibrated from bender element tests.
- m_T is a parameter that controls the initial shear modulus upon 90° strain path reversal. It can be approximated as 0.5 of m_R .
- R is the parameter that represents the elastic range in the stain space. It is a material constant.
- β_r, χ are parameters that control the rate of degradation of the stiffness with strain. They are also material constants.

Advantages

The model is capable of accumulating strain and pore pressure in response to cyclic wave loads. The model parameters are less in number and have their own physical meaning. It is commercially available in PLAXIS (FEM software in which the analysis is undertaken). It incorporates both hardening and softening behaviour of the sand. The Matsuoka-Nakai failure criterion is used which is more realistic than the Mohr-coulomb failure criterion. The stiffness dependency on relative density and mean stress is achieved.

2.5.3. HYBRID MODELS

Despite having the advantage of calculating the accumulation of strain caused by cyclic loading, the hypoplastic sand model failed to do the same in long-term. The main reason behind such a behaviour is the disadvantage of the implicit method. The numerical calculation by Finite Element Method (FEM) uses the implicit scheme where the $(\sigma - \varepsilon)$ constitutive model calculates the stress and strain each cycle. Therefore, the implicit method may increase the numerical errors when the number of cycles is greater than 50 [20][32][38]. Moreover, higher number of cycles also increase the necessity of computational resource. In order to arrive at a solution for such problems, researchers [7][20] attempted to use the explicit methods. Apparently, explicit methods also have some disadvantages such as resulting in significant errors. Thus, the researchers incorporated both the implicit & explicit methods in the name of hybrid models: The HCA model by Wichtmann (2005)[20] where they combined bochum accumulation model with the hypoplastic sand model; Pasten et al (2013) [32] incorporated the empirical strain accumulation function with classical constitutive models (modified cam clay); Lupea (2013)[7] incorporated empirical pore pressure accumulation with hypoplastic sand model. Eventually, they all behave in a similar manner that the implicit method is used for the initial 50 cycles followed by extrapolation (explicit method) and then again the implicit method is used to control the extrapolation which reduces the error propagation. The author suggests that the interested readers could consider the following literature to get the better idea [20].

In the above section, the constitutive models including both elastoplasticity and hypoplasticity that considers the cyclic behaviour of sand is discussed in detail along with their respective advantages and disadvantages. An overview of available hybrid models is also presented. Considering the advantages and the availability in the commercial finite element software such as PLAXIS, it is concluded that the hypoplastic sand model will be used in this thesis.

2.6. FACTORS INFLUENCING THE CYCLIC BEHAVIOUR OF THE SOIL

There are several factors such as void ratio, load characteristics that influence the soil behaviour. As explained in the above section 2.3, the response is significantly dependent on the drainage type of the soil domain. Thus, the cyclic behaviour of the soil is indirectly influenced by the factors that affect the drainage type. In order to validate the response of the model analysed, sensitivity analysis has to be done with these factors. Along with the support of literature, Long & Vanneste (1994)[42], Le Blanc(2005), Lupea(2013)[7], Christakos(2003)[43], it is inferred that the following factors influence the cyclic behaviour of the soil:

- Relative density,

It is well known that the shearing behaviour of the soil depends on it, say; dense sand dilates and the loose sand contracts during shear. The change in state changes the strength of the soil. Therefore, the cyclic behaviour is highly influenced by the state of the soil (void ratio).

- Loading characteristics (one-way or two-way),

The load characteristics is defined by two components of the wave called cyclic stress (τ_{cyc}) and average stress (τ_{avg}). The cyclic component is directly related to number of cycles required to induce liquefaction, whereas the average component affects the drainage behaviour in terms of settlement. Both the components influence the cyclic behaviour of the soil. Therefore, load characteristics of the wave is an important factor to be analysed to find the critical case.

- Frequency (time period of wave),

Frequency is inversely proportional to time. Thus, the frequency will inversely affect the time allowed for the pore-pressure dissipation process. In that regard, the effect of wave frequency should be analysed to conclude the critical case.

- Magnitude of load (operating conditions , extreme conditions),

It is well known that, the magnitude of load influences the cyclic behaviour of the soil. The load magnitude varies with respect to the condition, say; the storm condition encounters higher magnitude of load than the operating condition.

- Number of cycles.

Number of cycles is directly related to the cyclic behaviour of the soil.

2.7. CONCLUSION

This chapter reveals the design procedure in accordance with the international standard, DNV and also the limitations of the same in the case of cyclic loading is presented. The research that were attempted to optimise the design procedure by overcoming the limitations were clearly explained in each section. Moreover, constitutive models that take into account the behaviour of cyclic loading are explained. The important findings of this chapter is summarised below:

- The cyclic behaviour is complex to understand and the international standards acknowledge their limitations.
- The drainage type is an important factor that influences the cyclic response of the foundation.
- The failure envelope is proved to show the exact behaviour of the foundation without any discrepancy which the classical bearing capacity equation failed to do.
- The stress point is found to be inside the yield surface which exhibits the elastic deformation during the normal operation condition. Further, it reaches the yield surface and expand it during extreme loading condition which exhibits the plastic deformation.
- The hypoplastic sand model can be used to investigate the response of the pore pressure under GBS foundation to cyclic loads.
- In the context of monopiles, the cyclic response was found to increase the stiffness whereas, in the case of suction caisson, it showed only a minor change in stiffness. The accumulation in strain was found to happen in both foundations although the magnitude differed.

3

FINITE ELEMENT MODELLING OF THE GRAVITY BASED FOUNDATION AND THE SOIL DOMAIN

In this chapter, a brief summary of finite element calculations carried out on the Gravity Based Foundation (GBF) founded on sandy soil is presented. All finite element calculations are done using a commercial software called PLAXIS.

Initially, details about the foundation including simplifications made in the geometry are explained. Secondly, the constitutive model and their parameters which are used to model the soil domain is described. Thirdly, the loading strategy adopted to analyse this problem is presented. Fourthly, the mesh used to analyse the problem and their influence on the capacity is explained. Following which, the initial and boundary conditions of this problem are presented. Finally, the factors considered in this research to analyse the pore pressure behaviour is presented.

3.1. FOUNDATION

In order to concentrate in geotechnical issues and considering this research scope, the foundation is modelled as a stiff plate. Therefore, the structural failure is not considered in the whole calculation. Additionally, the bearing capacity in the X direction (global coordinate system) is neglected because the effect compared to the base bearing capacity is insignificant. The self-weight of the foundation plate is included in the ballast weight and therefore, it is set to zero in the material parameter data set. Material parameters of the foundation is given in the table 3.1.

Material	EA <i>kN/m</i>	EI <i>kN/m²/m</i>	ν -	w <i>kN/m/m</i>
Elastic	1.0E9	1.0E9	-	-

Table 3.1: Parameters of the foundation plate

Considering the limitation of a 2D model, the geometry of the foundation is simplified. The foundation is assumed to be infinitely long in the out-of-plane direction and thus, it is modelled in the plane strain model. Despite the assumption of infinite dimension in the Z-direction, loads are calculated for the foundation with a square base (that has the area similar to the circular base) and applied to the simplified geometry in the same way as the original geometry experiences. Thus, the results shown in upcoming chapters depicts the results of the foundation per unit length in the out-of-plane-direction. The wind load and the respective moment is applied at the sea bed. The simplified foundation along with the load applied on it is shown in the figure 3.1.

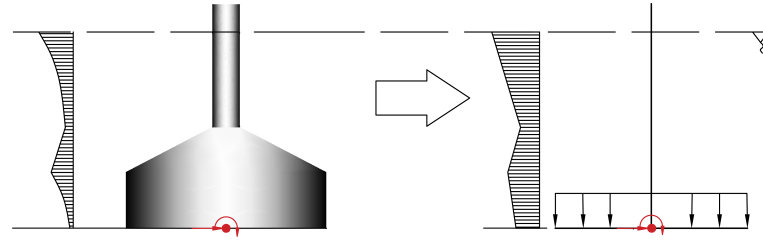


Figure 3.1: Simplified geometry of the foundation

3.2. CONSTITUTIVE MODEL

Material models that consider the pore pressure build-up and the strain accumulation during cyclic loading are presented in the previous chapter. Considering the advantages and availability, Hypoplastic sand model along with the inter granular strain concept is used in this Finite Element Analysis (FEA). Required soil parameters for the hypoplastic sand model are shown in the table 2.4 and for the intergranular strain concept in section 2.5.2. The sandy soil used in this research is Hostun sand [44][6] and their model parameters are shown in the table 3.2. Sand with different relative densities are considered in this analysis and they are dense sand (70%) and medium dense sand (53%). The initial void ratio is changed in accordance with the required relative density. Despite the change in relative density (initial void ratio), other parameters of the model remain unchanged. It is one of the advantages of the model that all parameters are same for a particular type of material and only the initial void ratio change representing different relative densities.

Symbol	Value	Units
ϕ_c	31	$^\circ$
h_s	1.0	GPa
n	0.29	–
e_{do}	0.610	–
e_{co}	0.960	–
e_{io}	1.090	–
α	0.13	–
β	2.0	–
m_R	5	–
m_T	2.0	–
R_{max}	$1.0E^{-4}$	–
β_R	0.5	–
χ	6.0	–
e_o	0.7510, 0.8310	–
R_D	70, 53	%

Table 3.2: Model parameters of the Hostun sand

3.3. LOADING STRATEGY

In order to predict a suitable loading strategy, several strategies are analysed. The validation of each of the methods is explained in this sub-section. The simplified geometry of the foundation and Hostun sand with relative density 70% are used to check the validity of loading strategies. The load applied adopts the asymmetric one-way mode of cycling ($\tau_a, \tau_{cyc} > 0$).

3.3.1. METHODOLOGY 1

The drainage type is one of the important parameters that influences the soil behaviour during wave loading. Therefore, the drainage type of Hostun sand with the expected frequency of loading is analysed by a method developed and validated by Zienkiewicz et al (1980) [29]. The method is:

$$\Pi_1 = \begin{cases} < 10^{-2} & \text{undrained} \\ \in [10^{-2}; 10^2] & \text{partially drained} \\ > 10^2 & \text{drained} \end{cases} \quad (3.1)$$

where,

$$\Pi_1 = \frac{2k}{\left(\frac{\rho_w}{\rho_s}\right) \cdot \pi \cdot g} \cdot \frac{T}{\hat{T}^2}; \quad \hat{T} = \frac{2L}{\sqrt{\frac{D+(K_f/n)}{\rho_s}}}; \quad D = \frac{E_s}{3(1-2\nu)}$$

and the parameters are,

Π_1 is the dimensionless number[-]

k is the permeability of the soil [m/s]

ρ_w is the density of water [kg/m^3]

ρ_s is the density of the soil [kg/m^3]

g is the gravity due to acceleration [m/s^2]

T is the time period of the wave [s]

\hat{T} is the natural period of the system [s]

L is the drainage length [m]

K_f is the bulk modulus of the fluid [kPa]

n is the porosity of the soil [-]

D is the bulk modulus of the soil [kPa]

E_s is the young's modulus of the soil [kPa]

ν is the poisson's ratio [-]

The detailed calculation of Π_1 is given in Appendix C. For the wave frequency of 0.1Hz, it is clear that the Hostun sand will not permit the drainage as the resulting value of Π_1 is $5 * 10^{-3}$. Therefore, the soil should be modelled in undrained condition. In the event of investigating the settlement in undrained soil caused by cyclic loads, Yildirim and Ersan (2007) [22] adopted a loading pattern invented by Yashura and Andersen (1989) and validated the same for undrained soils. According to Yildirim and Ersan, the wave load can be applied in a regular pattern as shown in the figure 3.2a. The wave load is applied in consecutive undrained plastic phases and following it the calm period (no wave load acts during the calm period) is modelled as the consolidation phase which allows the drainage. The same pattern is adopted in this case where the drainage is restricted for 10 consecutive cycles in each of the load packets (total period of wave activity = 100 s) and is allowed for 10 minutes in the calm period.

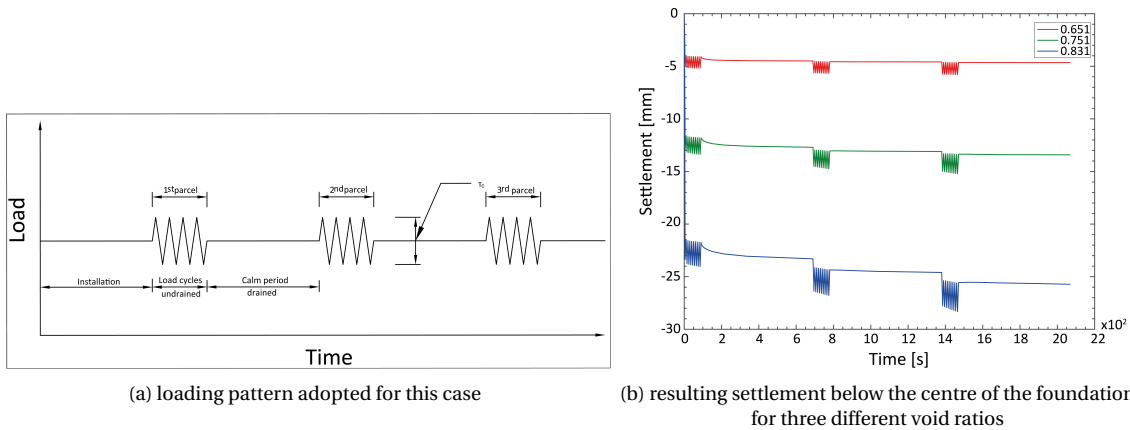


Figure 3.2: Loading strategy and the resulting settlement

The resulting settlement of the foundation is shown in the figure 3.2b. It is clear from the plot that the cyclic settlement keep on increasing for the case with void ratio 0.831. Such behaviour is because of the process called ratcheting [32]. Moreover, the overall trend is controlled by the calm period (post-cyclic behaviour) which is not the focus in this research. It is also worth noting that there are several discrepancies in this method as follows:

- The validity of the model used here is limited to linearly elastic domain and 1-D waves. Therefore, it may vary on extrapolation.

- Number of load cycles in a packet of cyclic load and the duration of the calm period are arbitrary assumptions.
- The whole trend is dominated by the calm period (post cyclic period) and thus it will be dependent on the assumed time period.
- The time effect is not taken into account since the plastic phase in Plaxis is time independent [45].

Therefore, it can be concluded that this methodology is not valid for this research.

3.3.2. METHODOLOGY 2

The frequency (time effect) is also an important parameter which influences the pore pressure behaviour [35]. In order to consider the time effect, the loading is modelled in consolidation phases. Each of the phases continue for a specified time period within which the given load is applied to the structure. Therefore, the pore pressure builds as well as dissipates in the same phase with respect to the time period allowed for that particular phase. It can be justified that the undrained behaviour of the Hostun sand is because of the 1-D waves and also it is valid only when the soil is linearly elastic (previous methodology). Therefore, the non-linear elastoplastic soil may behave partially drained on encountering waves in 2-D and 3-D conditions. With reference to research like Naves (2013) [11] and Lupea (2013) [7], the quasi-static cyclic load is applied as a box function. It is worth noting that the load applied by them acts in the vertical direction. The quasi-static load which is applied on the foundation is superimposed on the original wave load and shown in figure 3.3. In our case, the same strategy is adopted to model the load but it will act in the horizontal direction. The box function of the applied quasi-static load can be explained as follows:

- Phase 1: The maximum component of the cyclic load is applied in this phase and also the applied load sustains for a certain period of time in accordance with the frequency of the wave.
- Phase 2: The minimum component of the cyclic load is applied in this phase and also the applied load sustains for a certain period of time as the previous phase did.

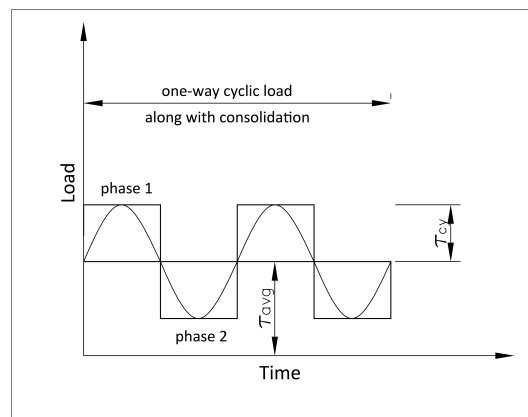


Figure 3.3: Loading pattern used in this analysis

This methodology takes into account both the time effect and the partial drainage condition. Therefore, it is used for this research.

3.4. MESH DEPENDENCY

The mesh used in this research is shown in the figure 3.4. The mesh is refined with a user defined coarseness factor and the factor is assumed from the results of the mesh dependency analysis. The refinement area is chosen based on the results [2.10] showing the failure surface generated within this area.

In order to finalise the coarseness factor for the refinement of mesh in the selected area, a mesh dependency analysis is done with various coarseness factors. The analysis is done on the sand with initial void ratio 0.7510 representing the dense sand (relative density : 70%). The safety analysis is done under the pure vertical load and the resulting factor of safety (FOS) for different coarseness factors are compared in the table 3.3.

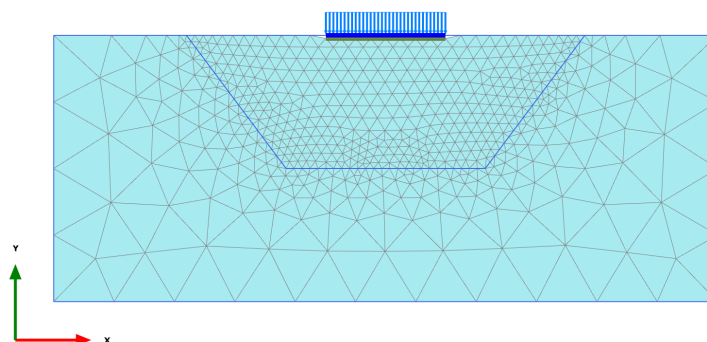


Figure 3.4: The generated mesh used in this analysis

Coarseness factor [-]	Number of elements [-]	Factor of safety [-]	percentile of deviation [%]
0.05	22882	4.01	0
0.1	6396	4.129	2.9
0.2	1876	4.103	2.3
0.25	1284	4.147	3.3
0.3	1070	4.150	3.4
0.4	802	4.159	3.6
0.5	592	4.225	5.1
0.6	466	4.226	5.1
0.7	420	4.233	5.3
0.8	338	4.222	5.0
0.9	284	4.317	7.0

Table 3.3: Factor of safety depending on the coarseness factor

It is evident from the table 3.3 that the increase in the overestimation of the capacity increases along with the coarseness of the mesh. Moreover, it also shows that the minimum coarseness factor 0.05 with number of elements 22882 represents the natural soil condition as much as possible. Unfortunately, the increase in number of elements also increase the calculation time, reducing the computational efficiency. Therefore, the author opts for the coarseness factor, which is able to represent the natural soil condition without having much deviation in terms of factor of safety. In the event of doing so, the coarseness factor 0.3 is chosen, despite having the FOS 4.150 which deviates 3.4% from the coarseness factor 0.05. Although the number of elements is decreased considering the percentile of deviation, the analysis incorporating the wave loads encounters convergence error. The stress singularities are observed at several stress points in the refinement area. Thus, the mesh is refined with the coarseness factor 0.25, which converges well capturing the stress locally at each point. It is also worth noting that, the FOS 4.147 of the selected coarseness factor deviates only 3.3% from the finest mesh possible (22882 elements). Therefore one can conclude to use the factor 0.25 that represents the natural soil condition.

3.5. INITIAL AND BOUNDARY CONDITIONS

3.5.1. INITIAL CONDITIONS

The soil domain is assumed to be homogeneous in nature which is a simplifying assumption. It is also worth noting that, the dimension of the foundation base in the horizontal direction is 36m, which will allow variability in the horizontal direction as well. Even then, the soil domain is assumed to be homogeneous considering the time constraints of this thesis.

Since the installation of the foundation is assumed to be carried out during the calm period, the installation phase is considered as the drained case. As the drainage is allowed during installation, the consolidation period is not considered after installation.

Additionally, the stress distribution in the soil domain is calculated using K_0 procedure, which involves the friction angle to calculate horizontal stress from vertical stress.

3.5.2. BOUNDARY CONDITIONS

- **Displacement:** The displacement boundary conditions are shown in the figure 3.5a. The bottom boundary is fixed to represent the bed rock. Thus, the displacement in both X and Y direction are restrained. The top boundary is free in both X and Y direction. Thus, the displacement occurs in all the direction. Both the side boundaries are fixed in the normal plane. Therefore, the displacement in X direction is restrained whereas the displacement in Y direction is allowed.

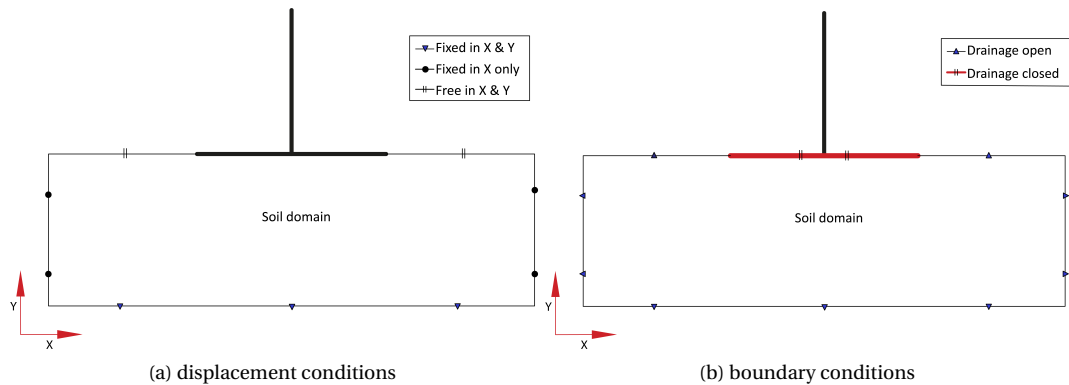


Figure 3.5: The boundary conditions for the soil domain used in this analysis

- **Drainage:** The drainage boundary conditions are shown in the figure 3.5b. All the three boundaries, except the top boundary representing the sea bed, are closed (do not allow the seepage of water) as the boundaries are away from the zone of influence. Even in the sea bed, the surface covered by the foundation base is closed because the concrete is impermeable.

3.6. FACTORS INFLUENCING THE CYCLIC BEHAVIOUR OF THE SOIL

The factors that will influence the cyclic behaviour of the soil are explained in the previous chapter and they are as follows,

- Relative density,
- Load characteristics of the wave,
- Wave frequency,
- Magnitude of load, and
- Number of cycles.

In this case, the influence of number of cycles is not studied as it is limited to 50 cycles. The literature reports that the implicit method used here may increase numerical errors when the number of cycle is greater than 50 [20]. Moreover, the storm condition is also not studied considering the scope of this research.

The remaining factors will be analysed in order to conclude a critical case. Eventually, the critical case will be used to study the pore pressure effect on the capacity of the foundation.

3.6.1. RELATIVE DENSITY

As explained in the section 3.2, two different relative densities (D_r), one representing medium dense (53%) and the other representing dense sand (70%) are analysed. The relative densities are determined by initial void ratios such as 0.8310 (medium dense sand) and 0.7510 (dense sand). They are analysed to find their influence on the pore pressure behaviour. Furthermore, the void ratio 0.8310 (representing medium dense sand with $D_r=53\%$) is used to analyse the influence of other factors.

3.6.2. LOAD CHARACTERISTICS

As explained in the previous chapter, the load characteristics is one of the factors that influence the cyclic behaviour of the soil. In general, four modes (load characteristics) of cyclic loading are applicable and they depend on two components of load; the cyclic stress, τ_{cyc} (cyclic component), and the average stress, τ_{avg} (average component). These components are depicted in figure 3.3. The modes of cyclic loading are as follows:

- Two-way symmetric: $\tau_{avg} = 0$ & $\tau_{cyc} > 0$,
- Two-way unsymmetric: $\tau_{cyc} \geq \tau_{avg} > 0$,
- One-way unsymmetric: $\tau_{avg} = \tau_{cyc} > 0$, and
- One-way unsymmetric: $\tau_{avg} > \tau_{cyc} > 0$.

The one-way loading is considered to be more critical than the two-way loading as it does not cross the zero stress. Therefore, three different ratios (τ_{cyc} & τ_{avg}) of one-way cyclic loads are chosen and analysed. They are $\tau_{cyc}/\tau_{avg} = 1$, $\tau_{cyc}/\tau_{avg} = 0.6$ and $\tau_{cyc}/\tau_{avg} = 0.3$. The load applied in each part of the foundation for wave frequency of 0.1Hz is given in the table 3.4

Foundation part	$\tau_{cyc}/\tau_{avg} = 1$ kN/m/m	$\tau_{cyc}/\tau_{avg} = 0.6$ kN/m/m	$\tau_{cyc}/\tau_{avg} = 0.3$ kN/m/m
Top cylinder _{Top}	30.22	22.665	15.11
Top cylinder _{Bottom}	1.86	1.395	0.93
Base cylinder _{Top}	6.59	4.943	3.295
Base cylinder _{Bottom}	5.74	4.305	2.87

Table 3.4: Magnitude of cyclic load (τ_c) for the wave frequency 0.1 Hz subjected by various parts of the foundation

These loads are calculated using the semi-empirical equation called Morison equation and the detailed calculation procedure is given in Appendix A. Even though the magnitude of wave load changed in accordance with the ratio between cyclic and average load, the wind load and the respective moment is kept unchanged throughout the analysis.

3.6.3. WAVE FREQUENCY

Alongside load characteristics, two different frequencies (0.07Hz and 0.1Hz) which are in the activity range of waves occurring in nature[3], are analysed to find their influence on the pore pressure behaviour. Additionally, it is also worth noting that the change in frequency also induces change in load as the Morison equation is dependent on the time period of the wave.

3.7. CONCLUSION

In this chapter, the detailed explanation of material parameters of both plate and soil used in this analysis are presented. Different load application methods were analysed and the strategy that will be used in this analysis is finalised. The mesh used in this research is presented which is determined by a mesh dependency analysis. The important conclusions made in this chapter are summarised as follows:

- Considering the limitation of a 2D model, the geometry of the foundation is simplified and load calculations are done accordingly.
- Relative densities of the Hostun sand used in this analysis along with the respective initial void ratio are presented.
- The load will be applied in the consolidation phase such that the pore pressure builds as well as dissipate in the same phase.
- Mesh dependency analysis revealed the coarseness factor which is used to refine the mesh in the selected area.
- The variation in factors influencing the pore pressure behaviour in the soil considered in this research are presented.

4

ANALYSIS AND RESULTS

In this chapter, a detailed discussion of results with respect to research questions obtained by analysing the model created in chapter 3 is presented.

Initially, the general description of stress state and stress points which act as the prerequisite for the discussion is given. Secondly, the stress behaviour in-terms of pore pressure and total stress at different stress points below the foundation are discussed. Thirdly, influence of factors such as relative density, load characteristics and wave frequency on the cyclic behaviour of soil with regard to pore pressure is discussed. Considering the conclusion, failure envelope on H-M space is developed for the foundation founded on the sand affected by 50 number of cycles, and their response to cyclic load is discussed. As the analysis mainly involve the consolidation phases, the influence of consolidation time period on the foundation capacity is analysed and discussed in the end.

4.1. GENERAL DESCRIPTION

4.1.1. STRESS CONDITIONS

Due to the fact that the mode of shearing is not same under the foundation, the soil tends to behave differently at various areas along a potential failure surface. Different shearing modes along the failure surface are presented in the figure 4.2. As seen, the soil at edges of the footing would replicate the simple shear behaviour whereas other areas would replicate the triaxial compression and extension behaviour.

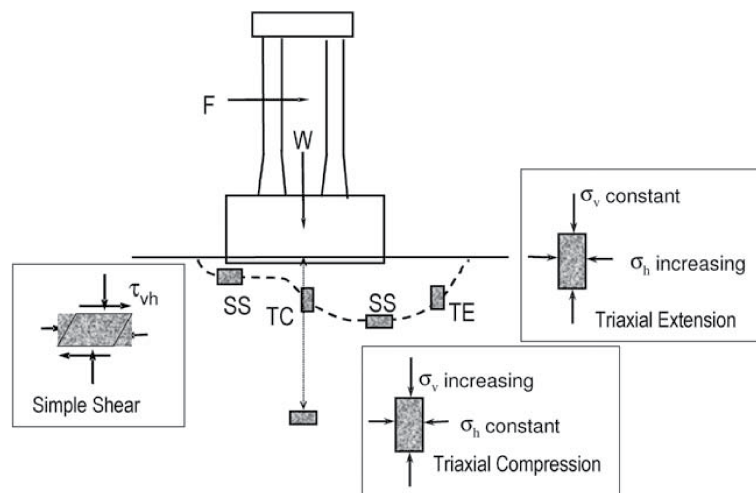


Figure 4.1: Anticipated stress state around the foundation [8]

4.1.2. STRESS POINTS

The behaviour of the soil is analysed on different stress points below the foundation. The coordinates of the stress points are as follows,

- L (-12.93, -1.28),
- M (-8.43, -1.28),
- N (-0.03, -1.75),
- O (8.38, -1.27), and
- P (12.87, -1.27).

The selection of stress points is based on the anticipated failure surface which go along different stress states as shown in figure 4.2 . The results discussed in this chapter represents the behaviour of above mentioned stress points and those points are shown in the figure 4.2

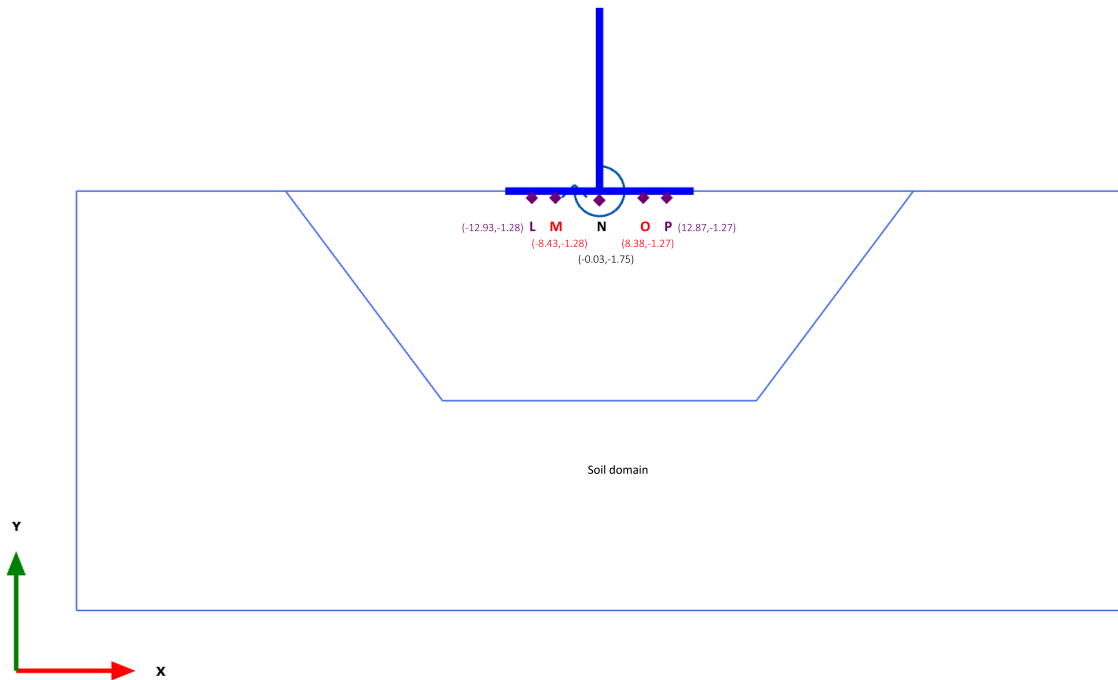


Figure 4.2: Stress points chosen for this analysis

4.2. STRESS BEHAVIOUR

4.2.1. PORE PRESSURE BEHAVIOUR

The applicability of the implicit method is restricted to 50 number of cycles as the probability for the accumulation of numerical errors is high [20]. Therefore, in this analysis, the number of cycles is restricted to 50 cycles. The pore pressure behaviour at different stress points is explained with the help of figure 4.4. The process of pore pressure development can be explained with respect to the phase involved. The process is shown in figure 4.3 and it is described as follows,

- During phase 1 (figure 4.3a), where the maximum component of the cyclic load is applied, negative excess pore pressure (EPP) develops on the right side of the foundation. This is because of the application of positive load.
- During phase 2 (figure 4.3b), where the minimum component of the cyclic load is applied (in this case it is zero as $\tau_{cyc} = \tau_{avg}$), the negative EPP on the top-right side of the foundation dissipates as the drainage distance is small, but the same develops on the left side of the foundation.

Therefore, at the end of the first cycle, the negative EPP remains undissipated on the left side and few meters below the right side of the foundation. The distance on the right side (where the negative EPP is dissipated) is influenced by two parameters and they are (1) time period of the wave and (2) drainage length.

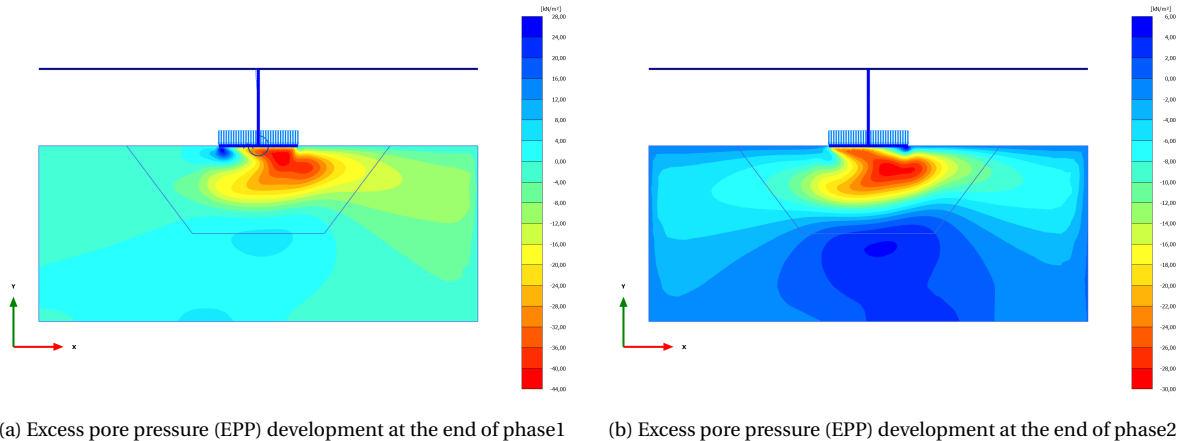


Figure 4.3: Pore pressure generated during each phase

It can be inferred from the figure 4.4 that, the middle of the foundation which has longer drainage length experiences maximum negative EPP in the initial stage. Nevertheless, as we progress through the cycles, it is seen not to be true as they are distributed to the edges of the foundation. At later stage, despite having a smaller drainage length, edges of the foundation (L&P) encounter negative EPP which is higher in magnitude because of the time period allowed for the dissipation and the tendency of water to move from high pressure to low pressure gradient. It can also be justified as the build-up in negative EPP becomes relatively insignificant at the centre point (N) when the number of cycle increase. However, irrespective of the stress point, the build-up in pore pressure is evidenced to decrease when the number of cycle increase. This is because of the process called densification [7]. Furthermore, the increase in transient response of pore pressure can be explained in relation with the total stress later in this section. In general, the magnitude of the negative EPP is higher at the left edge than the right edge of the footing as the soil dilate on the left edge (dense soil dilate during shear) whereas the other edge encounters compression due to high confining pressure (suppressed dilatancy).

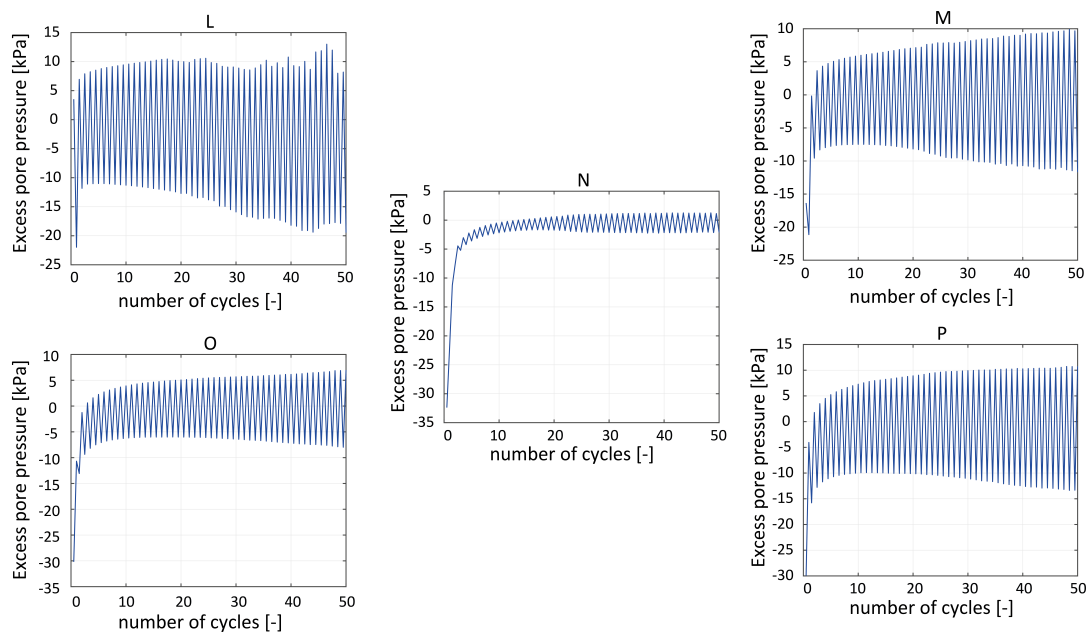


Figure 4.4: Pore pressure behaviour on medium dense sand ($D_r=53\%$)

4.2.2. TOTAL STRESS BEHAVIOUR

The total stress behaviour at different stress points is shown in figure 4.5.

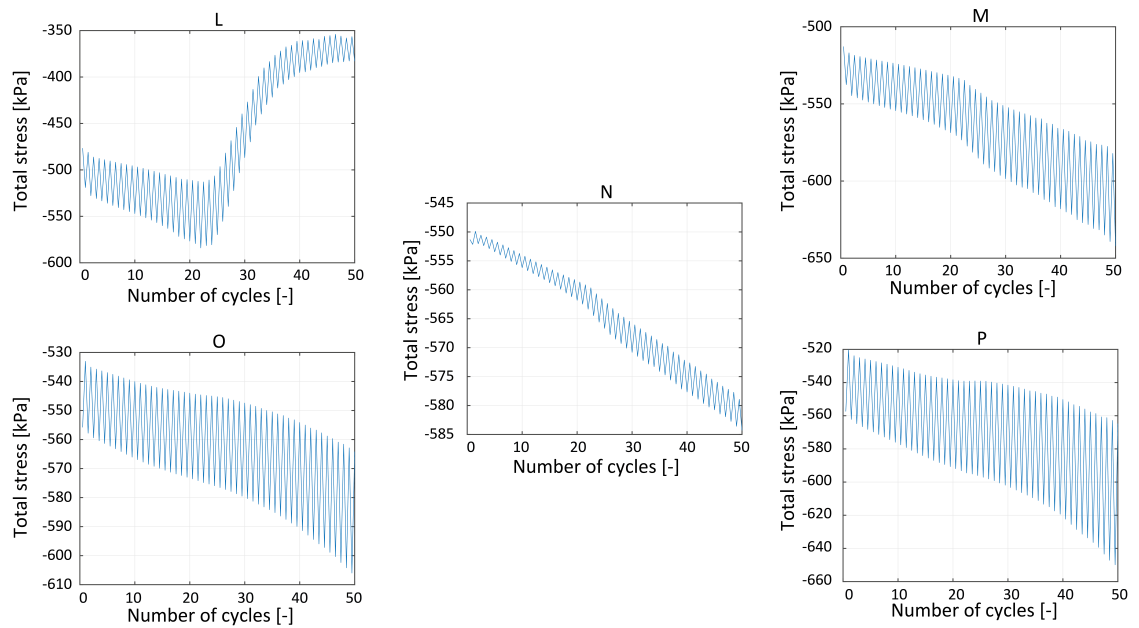


Figure 4.5: Total stress behaviour on medium dense sand ($D_r=53\%$)

As seen in figure 4.5, the total stress at stress point (L) reduces after 25 cycles because of the propagation of a failure surface and in response, the effective foundation area reduces as well. The reduction in total stress ceases on reaching the stress caused by hydrostatic pressure and static stress resulting from a metre of sand (sum of both in this case is around 380 kPa). Such ceasing behaviour is highly in-line with the reduction in effective foundation area. As the foundation plate considered here is a rigid plate, the foundation pressure will be high at the edges. Therefore, the rate of increment of total stress at M is increasing after 25 cycles as a result of change in effective foundation area. Similarly, despite having horizontal load acting towards the positive axis, the point M experiences higher total stress than the point O, which is at the same distance from centre but on the positive axis. This is also evidenced in negative EPP at the stress point M as shown in the figure 4.4 The increase in transient response of total stress goes hand in hand with the transient pore pressure as the mobilisation of soil strength happens in time. Furthermore, it is worth noting that the cyclic and average load is equal which helps in the consistent development of cyclic components of total stress and pore pressure. The propagation of failure surface can also be justified by the plastic deviatoric strain which increases after 25 cycles at the stress point L. The plastic deviatoric strain and the failure surface is shown in the figure 4.6.

4.3. INFLUENCE OF FACTORS ON CYCLIC BEHAVIOUR OF THE SOIL

The influence of aforementioned factors (3.6) on the cyclic behaviour of the soil is analysed and their results are discussed in this section with respect to the following sub-question. The sub-question is *How do factors such as Relative density, Load characteristics of the wave and the wave frequency influence the pore pressure behaviour?*. The results in this section will aid us to answer this question.

4.3.1. INFLUENCE OF RELATIVE DENSITY ON CYCLIC BEHAVIOUR

Relative density is an important parameter which will influence the pore pressure behaviour. It is well known that the probability of the pore pressure development is less when the relative density of the sand is high [7]. The figure 4.7 shows the pore pressure behaviour at stress points L and P, which is near to the edge of the footing. The behaviour at other stress points are shown in Appendix D. According to the figure 4.7, the dense sand ($RD=70\%$) is less affected by wave loads in terms of pore pressure. Thus, the development of cyclic component of the pore pressure is also less, despite the ratio between average and cyclic load being one.

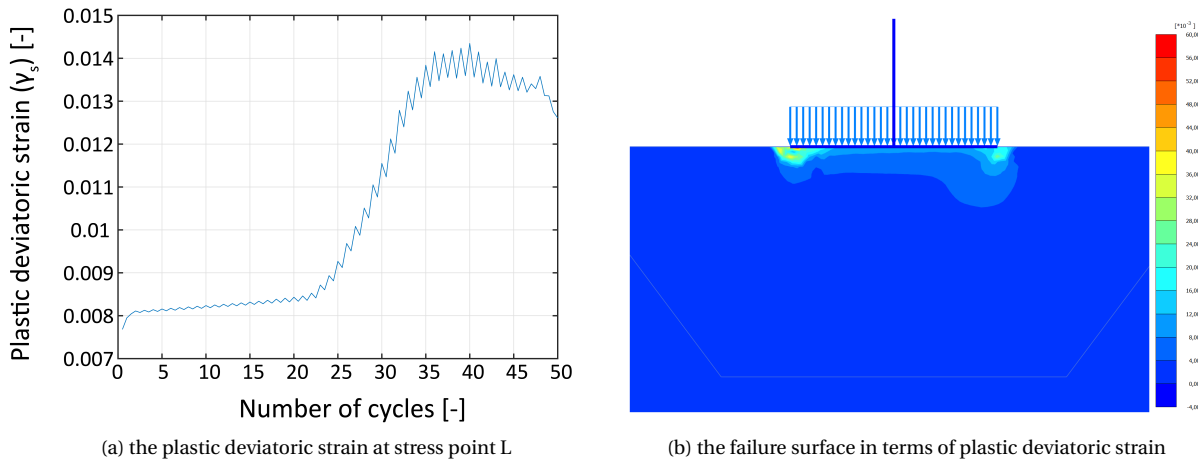


Figure 4.6: The development of failure surface

Therefore, it can be concluded that the medium dense sand (RD=53%) is significantly affected by cyclic loads which is in accordance with our understanding of cyclic behaviour of sand.

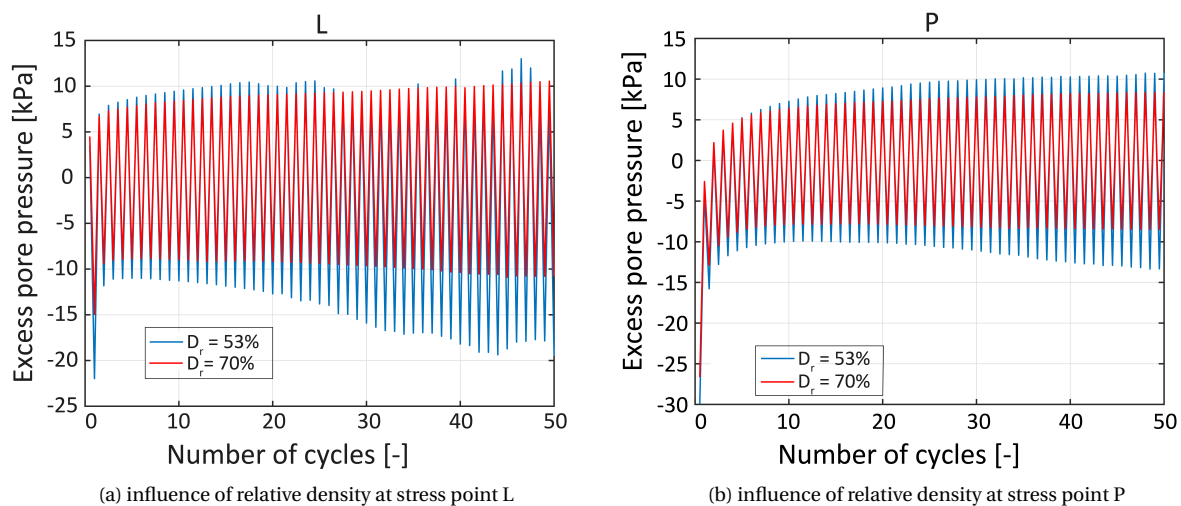


Figure 4.7: Pore pressure behaviour with respect to relative density

4.3.2. INFLUENCE OF LOAD CHARACTERISTICS ON CYCLIC BEHAVIOUR

As mentioned in 3.6.1, the medium dense sand is used to analyse the influence of load characteristics on the cyclic behaviour. According to the previous section, it is also more sensible to analyse the medium dense sand as it is significantly affected by cyclic loads. The figure 4.8 clearly depicts the load characteristics influence on the pore pressure behaviour. Similar to relative density, the behaviour is shown only from end points, L and P whereas other stress points are included in Appendix D

As shown in the figure 4.8, the development of EPP is rapid in the beginning which then dissipates irrespective of the ratio (τ_{cyc}/τ_{avg}). This is in-line with our understanding of pore pressure behaviour [35]. Initially, in terms of magnitude, the development of pore pressure in all cases is equal as they are subjected to the same load. However, at the end of the first cycle, the difference in EPP is evidenced with respect to the ratio between cyclic and average load. When the ratio (τ_{cyc}/τ_{avg}) is high, the transient response grows whereas the average response remains less. Therefore, the problem of stability can be caused by the degradation in cyclic shear strength [8]. When the ratio (τ_{cyc}/τ_{avg}) is low, indicating the increase in τ_{avg} , the response is vice versa. In this case, the problem of stability can be caused by the accumulation of strain (which will not be treated in this research).

Since the cyclic response of pore pressure is stronger during $(\tau_{cyc}/\tau_{avg}) = 1$, the strength degradation will be the predominant cause of the failure. Thus, it is concluded to be the critical case as the research focus is on the capacity of the foundation.

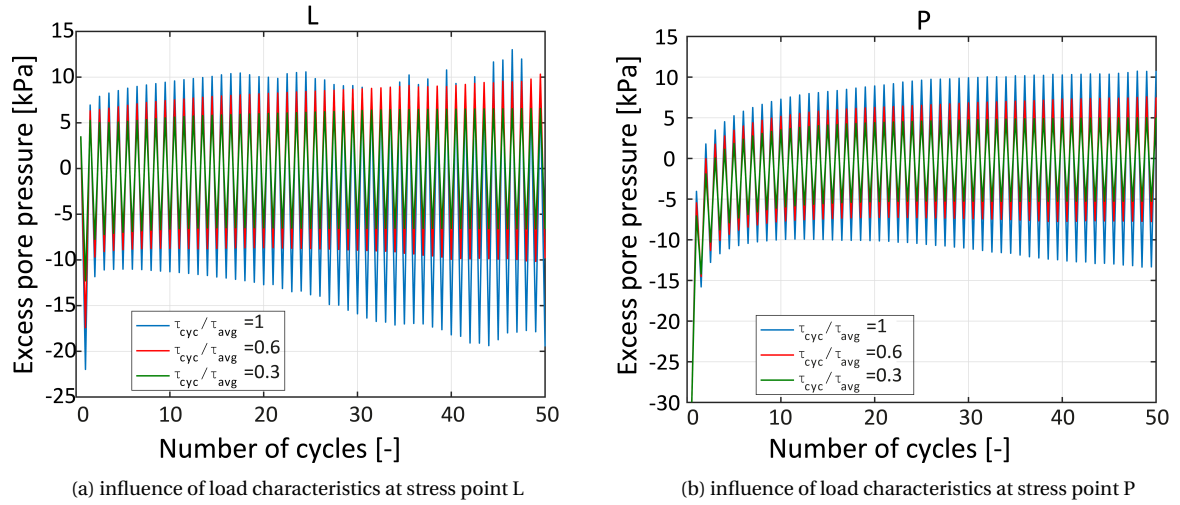


Figure 4.8: Pore pressure behaviour with respect to load characteristics

4.3.3. INFLUENCE OF WAVE FREQUENCY ON CYCLIC BEHAVIOUR

In order to investigate the influence of frequency, the medium dense sand with the load characteristics of $\tau_{cyc} = \tau_{avg}$ (one-way cyclic) is analysed, considering the conclusion from the above analysis. The influence of wave frequency on the pore pressure behaviour is shown in the figure 4.9. Apparently, similar to previous cases the behaviour is shown only at stress points L and P, and other cases are included in the appendix D.

The development of pore pressure is relatively higher at the initial stage for 0.1 Hz (higher frequency in our range [3]) as evidenced in figure 4.9. Although the dissipation happens in time, when the number of cycle increases, the excess pore pressure remains high. This makes sense as the case 0.1 Hz allows relatively less time for the pore pressure to dissipate. Therefore, as expected for 50 cycles, the higher frequency is found to dominate the influence on the cyclic behaviour significantly. The transient response in figure 4.9 indicates the rate of change in cyclic component (τ_{cyc}) of the load, which is again dominant in the case of 0.1 Hz.

In the end, 0.1 Hz which significantly influences the cyclic behaviour will be used to analyse the effect of pore pressure on the capacity envelope of the foundation.

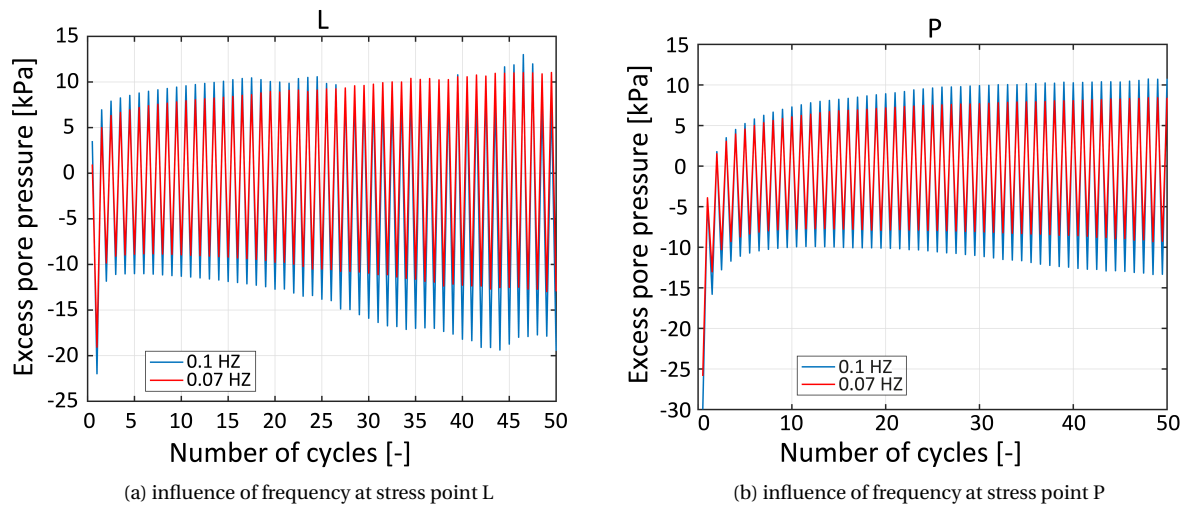


Figure 4.9: Pore pressure behaviour with respect to wave frequency

4.4. CAPACITY OF THE FOUNDATION

The study of factors that influence the cyclic behaviour of soil reveals that the sand with following properties will be significantly affected by the cyclic wave load. The critical case would be the medium dense sand (in this case RD= 53%) and it will be highly affected by the wave with frequency of 0.1 Hz. Therefore, it will be used in the analysis to investigate the effect of pore pressure on the capacity of the foundation. The cyclic strength properties of the soil would be significantly influenced by the load case in which $\tau_{cyc} = \tau_{avg} > 0$. Hence, it will be taken into account for the analysis of failure envelope as well. The reader should be aware that the critical case is defined only with respect to factors and characteristics that are considered in this research.

The effect of pore pressure on the foundation capacity is analysed for a critical case in the event of answering the main objective of this research, "What is the effect of pore pressure (due to cyclic loads) on the capacity of the foundation?". The results discussed in this section would form the basis to answer this question.

4.4.1. LIQUEFACTION POTENTIAL

In order to ensure that the foundation is safe with respect to liquefaction, the potential for it is analysed in terms of R_u in the critical case. Their results are presented in the figure 4.10.

R_u is the cyclic excess pore water ratio [46], defined as the ratio between pore pressure and initial effective stress [4.1],

$$R_u = \frac{\Delta u}{p'_{ini}} \quad (4.1)$$

Δu is the cyclic excess pore water pressure [kN/m^2]

p'_{ini} is the initial mean effective stress [kN/m^2]

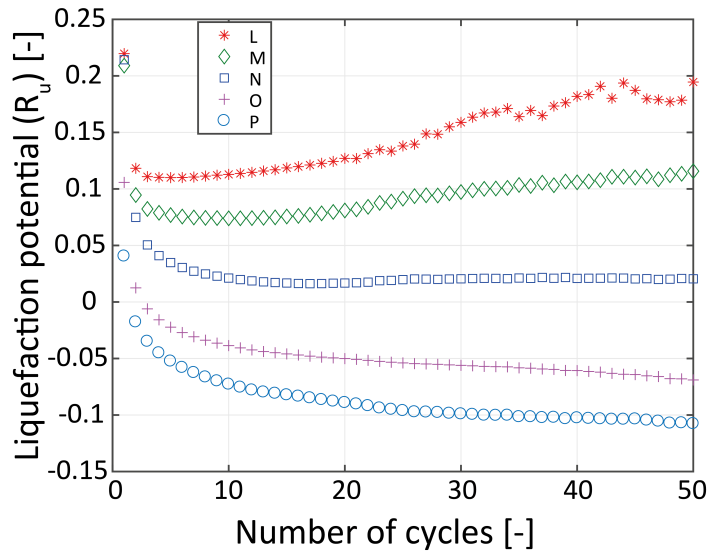


Figure 4.10: The potential for liquefaction failure at different stress points below the foundation

According to the equation 4.1, the value of 1 will be the lower limit at which the liquefaction will be initiated. It implies that the effective stress is completely replaced by the pore pressure.

As explained in section 4.2.1, the soil in the left edge of the footing dilates during shear. The voids created by dilation will be filled with water during the flow from high pressure to low pressure gradient. In figure 4.10, this process is acknowledged by the increase in R_u (at L). Even though the ratio increases, after 50 cycles it remains below 0.15, which is below the limit (1). The other points N,O,P in the figure 4.10 show the stabilization of the ratio and even reduction of the same, particularly in points at the right side of the foundation. This acknowledges the densification in the right side of the foundation, where the effective stress would be higher (also the liquefaction potential in dense sand is very less).

As a whole, the potential for liquefaction is insignificant under GBS and this emphasises that the foundation is safe after 50 cycles of wave loads. In this respect, one can conclude that the capacity of the foundation is

not going to decrease, atleast because of the liquefaction.

4.4.2. FAILURE ENVELOPE OF THE FOUNDATION IN H-M SPACE UNDER COMBINED LOADING

The analysis used to investigate the failure envelope of the foundation involves several sub-analysis with different eccentricities. Initially the vertical load is applied, following it the undrained plastic analysis is carried out with different eccentricities (H/M). Eventually, the undrained failure envelope in H-M space under working vertical load is created. The resulting H-M failure envelope is shown in figure 4.11, both H and M are divided by the base diameter (D) of the foundation.

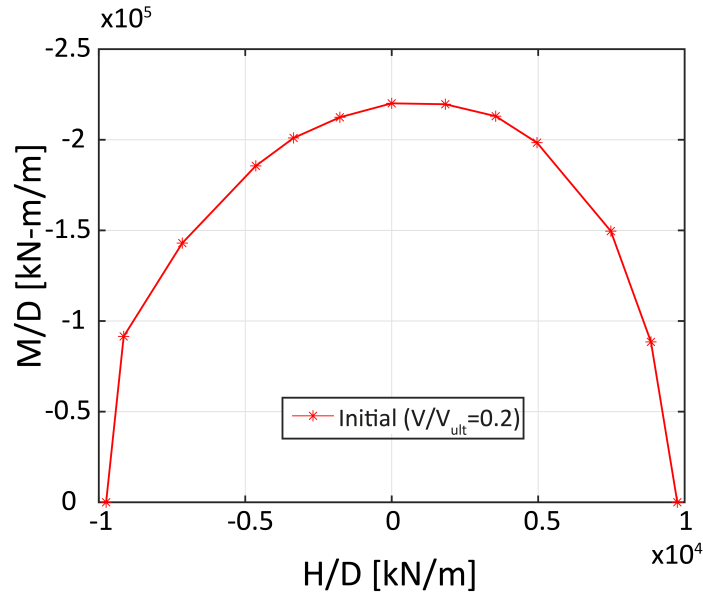


Figure 4.11: Failure envelope of our foundation in H-M space

The maximum moment capacity is mobilised when the foundation is subjected to a small horizontal load acting in the same direction as the overturning moment. It is observed that the shape of the failure envelope matches well with literature[15].

The sub-analysis revealed the failure mechanisms and they are presented in the figure 4.12. It is clear from the figure that the sliding failure mechanism governs the failure under pure horizontal loading (figure 4.12a) and toppling failure mechanism under pure moment load (figure 4.12c). Further, as the moment component increases, the horizontal component decrease with respect to the eccentricity. Therefore, the sliding failure mechanism transforms into a scoop-wedge mechanism. Eventually on mobilising the peak moment, the wedge develops on either side of the scoop defining wedge-scoop-wedge mechanism (figure 4.12b). The resulting failure mechanism matches well with results experienced by Gournvec [9] during the development of theoretical model that predicts the failure envelope under general loading. The results from Gournvec are shown in figure 4.13,

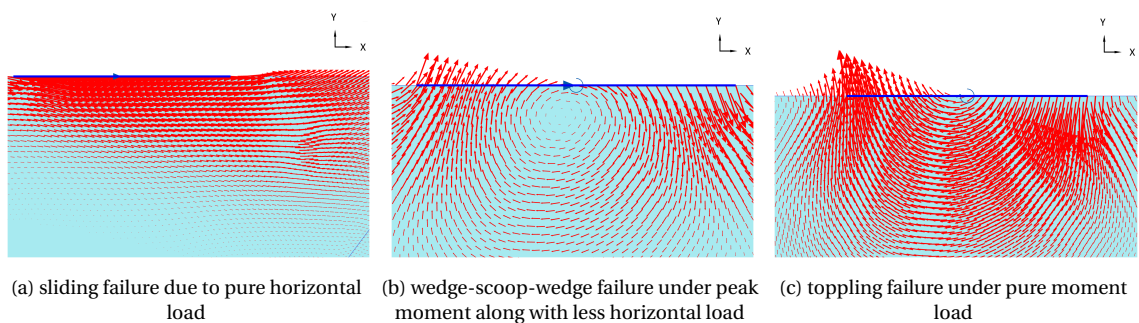


Figure 4.12: Failure surface generated under working vertical load

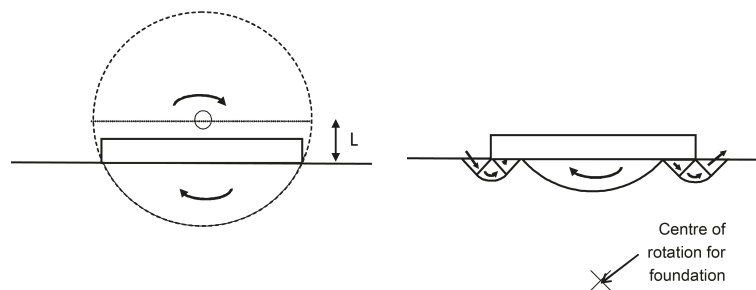


Figure 4.13: Failure surface experienced by Gournvec a) toppling (scoop) b) wedge-scoop-wedge [9]

4.4.3. INFLUENCE OF CYCLIC BEHAVIOUR OF SOIL ON H-M FAILURE ENVELOPE

In a similar way, the failure envelope in H-M space is developed with the soil affected by 25 and 50 cycles of the wave load and is shown in the figure 4.14.

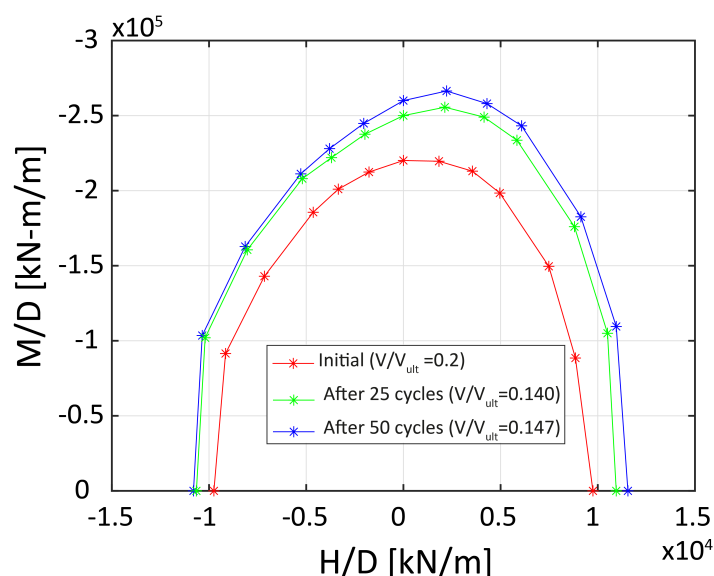


Figure 4.14: Effect of cyclic load on the capacity of the foundation

It is evident from the figure 4.14 that the failure envelope expands after 25 and 50 cycles of quasi-static wave load. Despite the build-up of negative EPP (resulting from cyclic load), the yield envelope expands. This same behaviour is evidenced after 25 cycles as well. The main reason behind such behaviour is densification that happens because of the consolidation and shearing behaviour of the medium dense sand [35]. The shearing behaviour depends on the confining pressure. Thus, dilation occurs on the left edge of the footing (where the confining pressure is less as the load acts on the right side) and compression occurs on the right edge of the footing (where the confining pressure is high). Moreover, the consolidation phase which is used here to model the quasi-static wave loads allows the sand to densify when the pore pressure is expelled (the expulsion of pore pressure reduce the volume of voids and increase the settlement). Apparently, such behaviour is in accord with the partially drained behaviour of the soil [47]. It is also worth noting that, Mangal [47] experienced the expansion in failure surface of the shallow foundation when the soil behaves as in a partially drained state.

The densification of the soil, increases the capacity of the soil and therefore, reduces the effect of pore pressure on it during the wave load (The analysis to study the influence of void ratio on cyclic behaviour revealed the same result). Eventually, the increase in capacity decreases the ratio V/V_{ult} (Initial $V/V_{ult} = 0.2$; After cyclic $V/V_{ult} = 0.15$), and thus increase the eccentricity of the peak (peak combination of H & M) [9][15]. Moreover, the expansion in failure envelope is also supported by the decrease in the ratio between working vertical load and the ultimate vertical load at the current state [9]. The figure 4.14 implies 15% (approximately) increase in the peak capacity after 25 cycles and 17% increase in the peak capacity after 50 cycle. This

proves that most of the expansion had happened at the 25th cycle indicating that the stabilisation of the cyclic behaviour of the soil is on the way. Thus, one can conclude that the failure envelope expands until a certain number of cycles after which the capacity remains same (or atleast the change is insignificant) during its life time.

Utilising the advantage of the hypoplastic sand model, a simple analysis is done in order to create the undrained failure envelope. The initial void ratio of the soil is changed to the void ratio that resulted in the soil affected by 50 cycles and then the failure envelope is developed. It is compared with the failure envelope after 50 cycles in the figure 4.15a. The influence of pore pressure that developed during 50 cycles will be one of the reasons for the reduced capacity.

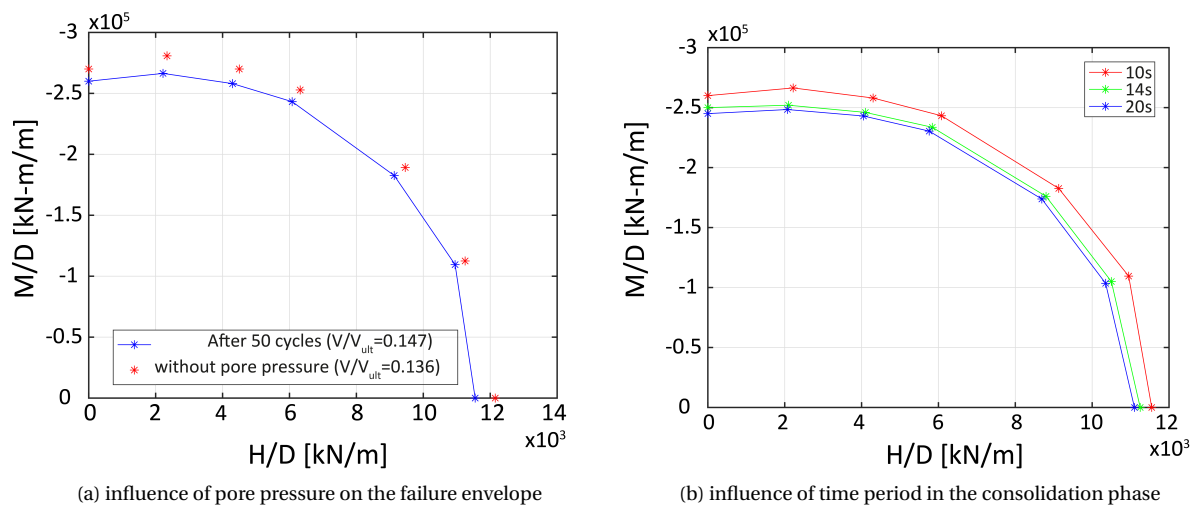


Figure 4.15: Comparison of failure envelopes

4.4.4. INFLUENCE OF TIME PERIOD IN CONSOLIDATION ON THE FAILURE ENVELOPE

In order to find the influence of load application rate, analysis with different time period in consolidation phase is done. The increase in size of the envelope with decrease in time period is evidenced as experienced by Mangal [47].

As shown in the figure 4.15b, the time period influences the failure envelope of the foundation due to the change in pre-consolidation stress of the soil. Since the hypoplastic sand model is based on incremental non linear stress rate - strain rate formulation, the effect of time period (creep effect) resulted in dominant pre-consolidation stress. If the time period is high, the dissipation of negative EPP will be high and this eventually results in high effective stress (say case 2 = 20s). If the time period is less, the response will be vice versa (say case 1 = 10s). In comparison, the pre-consolidation stress in the case 2 will be greater than the case 1 after the first cycle. Therefore, the case 2 requires large change in effective stress to overcome the pre-consolidation stress in upcoming cycles whereas the case 1 requires relatively less change in effective stress. It is also worth noting that, in case 1 (10s) more number of cycles will be applied at a particular time than case 2 (20s). The more frequent loading (increase in total stress) helps the case 1 to exceed the pre-consolidation stress more number of times as it requires a relatively small increase in effective stress to do so. The less frequent loading and the requirement of large change in effective stress prevents the case 2 to exceed the pre-consolidation stress as many number of times as the case 1 did. Eventually, the case 2 result in lesser capacity than the case 1. Therefore, it is concluded that the expansion in failure envelope is affected by the time period of the consolidation phase, which is used to model quasi-static wave loads.

4.5. CONCLUSION

In this chapter, the detailed discussion of results from the Finite Element Analysis in Plaxis is carried out. The important findings of this chapter will be summarized as follows.

- The stress state in the soil domain below the foundation is anisotropic and it is evidenced in this case as well [4.6b].

- The edges of the foundation experience higher negative excess pore pressure than the middle, despite having the smaller drainage length.
- The total stress reduces at the stress point L (edge of the footing) after 25 cycles because of the propagation of the failure surface.
- Analysing the factors which would influence the cyclic behaviour of the soil in terms of pore pressure, Medium dense sand (less relative density) under a wave of 0.1 Hz (high frequency) with one-way cyclic $\tau_{cyc} = \tau_{avg}$ load is found to be critical.
- The resulting failure surface is compared with the literature.
- The failure envelope of the foundation is found to be expanding in response to the cyclic load. The expansion is justified with the densification happening in the soil domain.
- The influence of the time period in consolidation phase is analysed which helps to conclude that the expansion in failure surface is significantly affected by the consolidation time periods.

5

CONCLUSIONS AND RECOMMENDATIONS

Results that are discussed in the previous chapter help to form the answer for the research question. Research questions along with respective findings will be presented in this chapter. Furthermore, the chapter concludes with recommendations for future work.

5.1. CONCLUSIONS

The ultimate objective of this research is formulated in the form of the main research question as follows,

What is the effect of pore pressure (due to cyclic loads) on the capacity of the foundation?

In order to answer this question two sub-questions were formulated and they are,

1. *How should the GBF be designed in accordance with the current generation guidelines and how the effects of cyclic loads are considered in it?*

By answering this question, the necessity of this research is realised. Furthermore, the advantage of using the failure envelope to investigate the cyclic load effects is emphasised. The answer is given in sub-section 5.1.1.

2. *How do factors such as Relative density, Load characteristics of the wave and the wave frequency influence the pore pressure behaviour?*

In the event of answering this question, a critical case among the considered characteristics that is most affected by cyclic loads is figured. Thus, the failure envelope for such case can be developed in order to examine the cyclic load effects. The answer for this question is given in the sub-section 5.1.2.

As said earlier, after answering the sub-questions, the main question is answered in the sub-section 5.1.3.

5.1.1. SUB-QUESTION 1

How should the GBF be designed in accordance with the current generation guidelines and how the effects of cyclic loads are considered in it?

- DNV [2][13], an international standard is used to design the Gravity Based Foundation (GBF). They deal with both Ultimate Limit State (ULS) and Serviceability Limit State (SLS), which are considered to be the important limit states of the foundation.
 - They provide the clear procedure for issues such as bearing capacity (Brinch Hansen equation), the sliding resistance (sliding criterion), and dynamic stability conditions. Moreover, they also help in settlement calculations, in particular, the immediate and consolidation settlement.

- Although it was acknowledged that the influence of cyclic loads should be considered in settlement calculation, they failed to explain the assessment procedure for cyclically induced settlement.
- However, they presented the procedure for assessing pore pressure accumulation based on the pore pressure contour plots but it involves several site specific laboratory tests, which is of less interest for industries.
- Further, with the help of Eurocode: EN-1997 [48], the rotational stability of the foundation is assessed.
- It is observed from both the standards that they concentrate more on static conditions. Although the dynamic stability is addressed in DNV, it concentrates only on estimating the foundation stiffness in order to avoid the resonance condition as explained in the section 2.2.4.
- Since the standards are found to have less concentration in the cyclic response, it can be concluded that a step towards understanding the cyclic response can further help in optimisation of the foundation making it cost efficient.
- Furthermore, it is also worth noting that, the research like Bransby & Randolph [27] and Gourvenec [9] proved that the classical bearing capacity equation underestimates the capacity of the foundation under general loading.
 - Initiating the first step, they invented a new concept called failure envelope which defines the optimised capacity.
 - Therefore in this research, failure envelope is developed which is then used to analyse the effect of cyclic loads on the same.

5.1.2. SUB-QUESTION 2

How do factors such as Relative density, Load characteristics of the wave and the wave frequency influence the pore pressure behaviour?

The influence of factors are analysed to conclude a critical case which will be most affected by cyclic wave loads. Following it, the capacity envelope will be developed for that critical case.

The influence of factors are as follows:

- *Relative density:* It is found that the sand with higher relative density remain less affected by the cyclic wave loads. This is because of the reduced void ratio which doesn't allow the pore pressure behaviour as allowed by sand with lower relative density. Therefore, medium dense sand (sand with relatively less density) is considered in this research.
- *Load characteristics:* The ratio between τ_{cyc} & τ_{avg} affects the pore pressure behaviour. Although, τ_{avg} can influence the stability of the structure during cyclic loading in-terms of settlement, τ_{cyc} is found to have more influence on the properties of the soil. In particular, when τ_{cyc} increases, the degree of influence also increases. Therefore, the case with $\tau_{cyc} = \tau_{avg}$ is concluded to have significant effects on the pore pressure behaviour.
- *Wave frequency* The results show that the influence of high frequency wave is more significant. As the frequency is inversely proportional to time, the high frequency wave allows less time for the dissipation of excess pore pressure. Therefore, the residual excess pore pressure is relatively higher in high frequency wave than the low frequency wave. And so, the high frequency wave will be considered as the critical case in this research.

The critical case can be defined by summarizing the above results as follows,

The medium dense sand affected by high frequency wave in which $\tau_{cyc} = \tau_{avg}$ will be the critical case. To summarise, the relative density considered here for the critical case is 53% and the wave frequency is 0.1 Hz (10 s).

It is stressed again that the reader should be aware of the critical case as it is defined here only with respect to the factors and characteristics that are considered in this analysis.

5.1.3. MAIN QUESTION

What is the effect of pore pressure (due to cyclic loads) on the capacity of the foundation?

Using the hypoplastic sand model, the effect of pore pressure on the failure envelope of the foundation is investigated. It has been found that cyclic loads have the significant effect on the foundation capacity when it is founded on the soil, which behaves partially drained during cyclic loading. The main findings are as follows:

- The undrained capacity of the foundation is found to increase after cyclic loading and the increase is justified by the process called densification. In this case, the magnitude of increase is reported to be 15% after 25 cycles and 17% after 50 cycles.
- The reduction in capacity due to negative excess pore pressure is witnessed in figure 4.15a. The resulting failure envelope (fig:4.15a) is developed for the same foundation, that is founded on the soil for which the initial void ratio equals the void ratio of the soil affected by 50 cycles of wave load.
- In comparison between figure 4.14 and 4.15a, it is clear that the densification effect overcomes the effect of pore pressure.
- The consolidation phase which is used to model the load is evidenced to control the expansion of the failure envelope as well.

In general, it can be concluded that the expansion in the undrained capacity of the foundation is evident when the soil is affected by the quasi-static wave load. The important aspect of this research is to obtain an insight on the capacity behaviour of the foundation when it is founded on partially drained soil. Therefore, the quantification of the expansion cannot be considered further to develop a general expression which can be used in the design guidelines. Moreover, the consolidation phase is also found to influence the magnitude of expansion.

5.2. RECOMMENDATIONS

As mentioned earlier, this dissertation aims to shed light on the behaviour of failure envelope under general loading in response to cyclic loads, but there are several other recommendations that can help to simplify the design guidelines taking into account the cyclic response. The recommendations from the author's perspective which would help to overcome the limitations of this research are presented as follows:

- A numerical model should be developed that takes into account the dynamics of the structure and dynamic wave load rather than the quasi-static wave load. Further, the partially drained behaviour of the soil can be incorporated in the model which will help to overcome the influence of the consolidation phase.
- The effect of settlement is not yet studied as the hypoplastic sand model failed to capture the shake down behaviour of the soil in response to cyclic load. This may pose serious consequences to the stability of structure under SLS.
- This dissertation concentrated on both medium dense and dense sand whereas the behaviour in loose sand remains unexplored. The potential for liquefaction in loose sand may be less because of the partially drained behaviour. Therefore, it is also worth investigating the response of failure envelope in loose sand.
- Importantly, this study involves only the load case of operating condition. Even though the author is aware that the magnitude of load is one of the important factors that affects the pore pressure behaviour, the storm conditions (where the magnitude of load rise naturally) are not considered here because of the time constraints. Thus, it is highly recommended to investigate the failure envelope response in storm conditions where the probability for pore pressure build-up is high.
- Although we have promising results with the physical reasoning behind each behaviour it is always recommended to validate results with either physical modelling or real cases.
- The wind load is considered to be the static load, therefore it can also be coupled with the wave load dynamically. This would provide the exact scenario as encountered by the real life wind turbines.

- The change in buoyancy force as the result of cyclic wave loads can also be taken into account for the optimisation.

A

APPENDIX

The environmental loads such as wind and wave load are calculated in accordance with Van Wijngaarden (2017) [35] and the Morison equation. The calculation procedure is explained in this appendix.

A.1. WIND LOAD

The wind load can be derived from the thrust force on the wind turbine, which is directly proportional to the square of the wind speed. The wind speed will be fluctuating throughout the lifetime of the wind turbine and thus using kaimal spectrum, a spectrum of wind loads can be derived to represent the actual loading conditions. Since waves have the major influence in pore pressure build-up [35], wind load for a maximum wind speed is calculated and used in this analysis ensuring the conservativeness. The thrust force can be calculated using the equation A.1.

$$F_{thrust} = 0.5 * \rho * A * C_T * U^2 \quad (A.1)$$

where,

F_{thrust} is the thrust force on the wind turbine [N]

ρ is the density of the air [kg/m^3]

A is the rotor swept area [m^2]

C_T is the thrust co-efficient [-]

U is the 10 minute average wind speed at the hub level [m/s]

The thrust co-efficient is an important parameter representing the dynamic behaviour of blades, but in this case as the thrust force is calculated for the maximum wind speed, the upper limit of the co-efficient [35] is calculated using the equation.

$$C_T = \frac{3.5 * (2 * U - 3.5)}{U^2} \quad (A.2)$$

Using the assumptions from table 2.3 and the above formula, the wind load can be calculated for our case.

A.2. WAVE LOAD

The waves in the sea is caused by the wind. Therefore, the waves can be seen in almost all the direction when the sea surface is examined. In order to account for these waves, several simplifications were made to find the elevation of a particular point with respect to time. Once the sea surface elevation with respect to time is achieved, it can be converted into a wave spectrum which then can be converted into individual sinusoidal waves. Those sinusoidal waves helps in estimating the wave particle kinematics. When the fully developed seas states for a particular wind condition is not available, several wave spectrum such as Pierson-Moskowitz and JONSWAP can be used.

In our case, as a first order approximation, a wave spectrum is created along with the assumptions, in accordance with the German standard Germanischer lyod [49]. This is clearly explained in the following sections.

A.2.1. DESIGN WAVE HEIGHT AND WAVE PERIOD

The assumptions for the site conditions used in this particular case is given in the table 2.3. The significant wave height is defined as the mean of the 1/3 highest waves in time series [49]. A simplification of the extreme design wave height for a 3 hour storm condition can be obtained from the equation A.3

$$H_d = 1.86 * H_s \leq H_b \quad (A.3)$$

where,

H_s is the significant wave height [m]

H_b is the breaking wave height [m]

The design wave height obtained using the equation A.3 is valid about 1000 waves. Moreover, it should be noted that, the design wave height must be smaller than the breaking wave height which is approximately 0.78 times the water depth.

Another important parameter, design wave period is difficult to estimate directly by measurements. Therefore, an empirical relation is given in the equation A.4.

$$11.1 * \sqrt{\frac{H_s}{g}} \leq T_d \leq 14.3 * \sqrt{\frac{H_s}{g}} \quad (A.4)$$

where,

g is the gravity due to acceleration [m/s^2]

A.2.2. WAVE LENGTH

The wave length of the design wave can be obtained implicitly using the equation A.5 in accordance with the international standard, DNV

$$\lambda = \frac{g}{2\pi} * T^2 * \tanh \frac{2\pi * d}{\lambda} \quad (A.5)$$

Considering the time constraint, a simple explicit approximation as given in [11] is used.

$$\lambda = \frac{2 * T^2}{2\pi} * \left[\tanh \left(\left(\frac{2\pi \sqrt{d}}{T} \right)^{3/2} \right) \right]^{3/2} \quad (A.6)$$

where,

T is time period [s]

d is depth [m]

A.2.3. WAVE PARTICLE KINEMATICS

For every harmonic wave extracted from wave spectrum, the wave particle motion can be described by linear wave theory according to Airy [10]. In the case of deep water ($\lambda > 0.5d$), the water particles move in circles in accordance with the harmonic wave. Moreover, the diameter of the circle decay with respect to depth below the surface as shown in figure A.1. In the case of intermediate depth ($0.05d < \lambda_{wave} < 0.5d$), the circular motion will shift to elliptical motion as an effect from seabed.

The linear wave theory assumes that the water particle velocity and acceleration is dependent on the wave amplitude. The velocity and acceleration of the water particle in the horizontal direction can be described by the equation A.7 with Z-axis pointing upwards from free surface.

$$\begin{aligned} u(z, t) &= \zeta * \frac{2\pi}{T} * \frac{\cosh k(z+D)}{\sinh kd} * \sin \frac{2\pi * t}{T} \\ \dot{u}(z, t) &= \zeta * \left(\frac{2\pi}{T} \right)^2 * \frac{\cosh k(z+D)}{\sinh kd} * \cos \frac{2\pi * t}{T} \end{aligned} \quad (A.7)$$

where,

ζ is the wave amplitude ($0.5 * H$) [m]

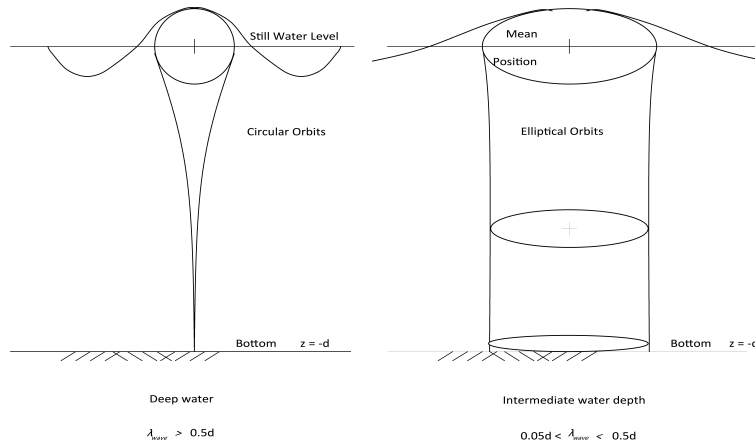


Figure A.1: Particle orbit in accordance with Airy theory [10]

H is the wave height [m]

k is the wave number $k = 2\pi/\lambda$ [-]

λ is the wave length [m]

T is the wave period [s]

D is the water depth [m]

t is the Time [s]

The wave particle motion in the horizontal direction at still water level ($Z=0$) for our case is shown in the below figureA.2.

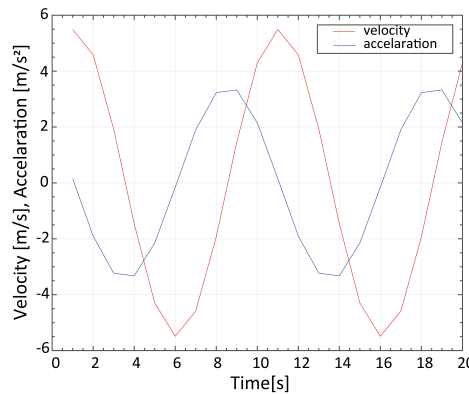


Figure A.2: Water particle velocity and acceleration in horizontal direction at the still water level

A.2.4. MORISON EQUATION

The Morison equation predicts the wave force per unit length of the structure called inertia and drag force. The inertia force is driven by the acceleration of the wave and the drag force is driven by wave speed. Thus, the wave particle kinematics are used to calculate the load on the structure.

$$\begin{aligned}
 f_{morison}(x, z, t) &= f_{drag}(x, z, t) + f_{inertia}(x, z, t) \\
 f_{drag}(x, z, t) &= C_d * 0.5 * \rho_{water} D |u(x, z, t)| u(x, z, t) \\
 f_{inertia}(x, z, t) &= C_m * 0.25 * \rho_{water} \pi D^2 \dot{u}(x, z, t)
 \end{aligned}
 \tag{A.8}$$

where,

f_{drag} is the hydrodynamic drag load [kN/m]

$f_{inertia}$ is the hydrodynamic inertia load [kN/m]

C_d is the drag coefficient [-]

C_m is the inertia coefficient [-]
 ρ_{water} is the density of water [kg/m^3]
 u is the water particle velocity [m/s]
 \dot{u} is the water particle acceleration [m/s^2]
 D is the diameter of of the cylinder section [m]

The validity of the equation is limited to small cylinders with wavelength ($\frac{\lambda}{D} > 5$). In order to improve the validity, Mac camy-Fuchs correction is used to determine the inertia co-efficient C_m based on the ratio D/λ_{wave} . The correction is based on the experimental data and it is shown in the figure A.3

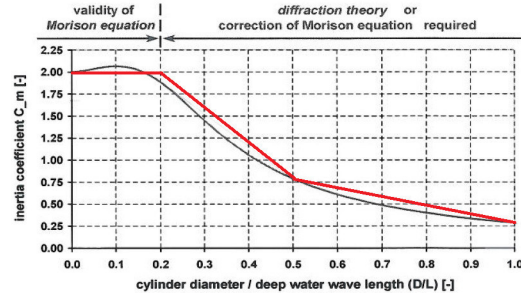


Figure A.3: Mac camy-Fuchs correction for the inertia coefficient C_m [11]

Resulting forces from the equation for our case is shown in the figure A.4.

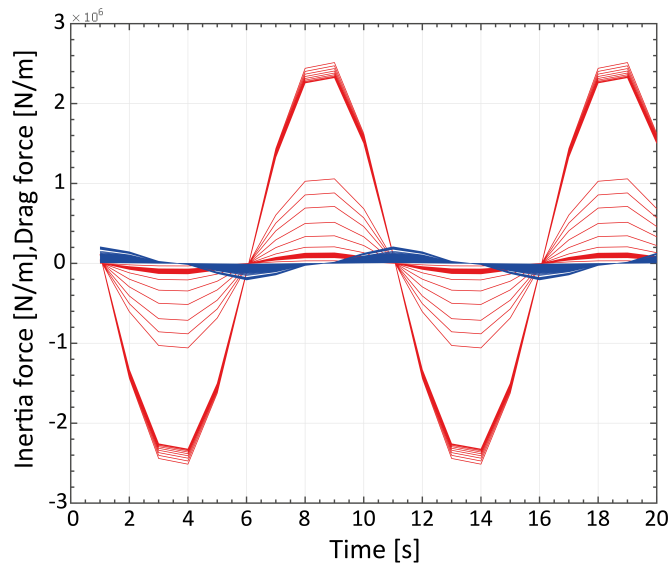


Figure A.4: Inertial and drag forces resulting from morison equation

It is clear from the above figure A.4 that the inertia force is dominating the drag force, as it is exponential to the cylinder diameter, where as, the drag force is linear to the cylinder diameter. Moreover, they both are in out of phase because of the behaviour of velocity and acceleration.

The horizontal load with respect to depth is shown in the figureA.5. The maximum load is taken into account for the analysis in order to have a conservative design.

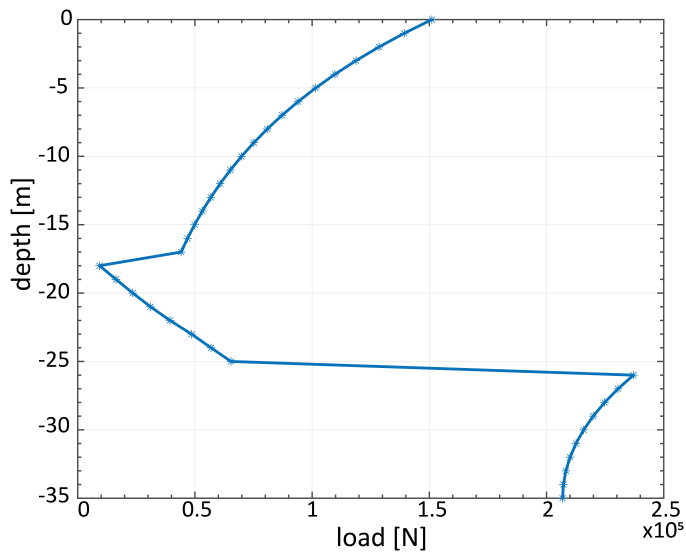


Figure A.5: Maximum horizontal hydrodynamic load resulting in the foundation

B

APPENDIX

A base case foundation supporting a 5 MW wind turbine is used in this analysis to find the effect of pore pressure. It is designed in accordance with the design basis as explained in the chapter 2 [2.2]. The stability check under Ultimate Limit State is explained in this appendix.

B.1. BASE CASE FOUNDATION DIMENSION

A clear description of dimensions are given in chapter 2. As a summary, figure B.1 showing their dimension is presented here.

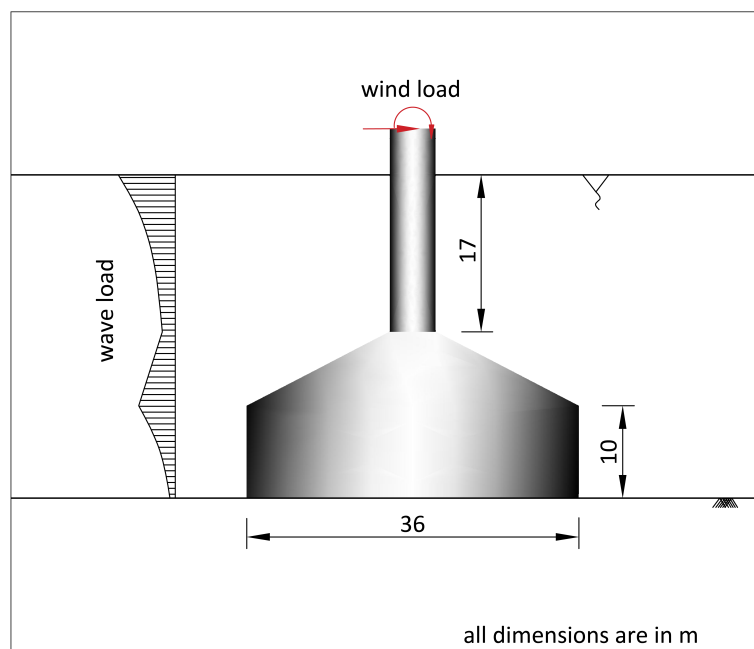


Figure B.1: Base case foundation used in this analysis

B.2. BEARING CAPACITY

The wind load along with the wave load that act in the horizontal direction will produce the moment on the base of the foundation. Thus, the eccentricity which reduces the effective area of the foundation is calculated as,

$$e = \frac{M_d}{V_d} = \frac{610078.7}{138110.5} = 4.4m \quad (\text{B.1})$$

Parameter	Value	Units
Effective area (A_{eff})	703.05	m^2
Effective length (L_{eff})	30.05	m
Effective breadth (B_{eff})	23.39	m
Bearing capacity factors $N_q, N_c \& N_\gamma$	43.40, 56.09 & 64.10	–
Shape factors $S_q, S_c \& S_\gamma$	1.47, 1.47 & 0.77	–
Shape factors $i_q, i_c \& i_\gamma$	0.84, 0.84 & 0.79	–
Effective unit weight (γ') (submerged)	11	kN/m^3
Design bearing capacity (q_d) (factored)	4249358.4	kN

Table B.1: Step by step calculation for the bearing capacity

Parameter	Value	Units
Interface factor (R_{int})	0.67	–
Interface friction angle δ_d	24.8	$^\circ$
Vertical load (factored)	138110.5	kN
Design sliding resistance	63954.8	kN

Table B.2: Step by step calculation for the sliding resistance

Furthermore, in accordance with DNV, the effective area is calculated and following it, bearing capacity for the drained sand is calculated and their steps are presented in the table B.1. Formulae used for the bearing capacity can be evidenced in the chapter 2.

The vertical load is considered to be unfavourable and thus, the factored vertical load is $207165.8kN$. The unity check reveals the ratio between the design load and the design resistance and that is 0.05

B.3. SLIDING RESISTANCE

Since, the wind and wave load act in the horizontal direction, it is mandatory to do a sliding check. The calculation of the resistance is shown in the table B.2

In this calculation the horizontal load is considered to be unfavourable and therefore, the design horizontal load is $12876.2kN$. The unity check reveals the ratio between the design horizontal load and the design sliding resistance which is 0.20

B.4. ROTATIONAL CHECK

The eccentricity of the load should not exceed 1/3 of the foundation width or 0.6 times the radius of a case of circular foundation (NEN 9997-1). Following it, a critical rotational check is also performed by assuming the point of rotation to be in the toe of the foundation. Calculations performed under this category is presented in the table B.3.

It can be incurred from the table B.3 that the unity check for eccentricity is 0.4 and the unity check for the critical rotation is 0.25.

Parameter	Value	Units
0.6*radius	0.67	m
Eccentricity	4.4	m
Moment load (factored)	610078.68	$kN - m$
Vertical load (factored)	138110.5	kN

Table B.3: Step by step calculation for the rotational check

From the above calculations, it can be concluded that the foundation used in this analysis is safe and conservative.

C

APPENDIX

A sample calculation for the drainage type investigation in accordance with the 1-D model by Zienkiewicz et al (1980) [29] is presented in this appendix.

In order to have the completeness, the model used to assess the drainage type is presented below,

where,

$$\Pi_1 = \begin{cases} < 10^{-2} & \text{undrained} \\ \in [10^{-2}; 10^2] & \text{partially drained} \\ > 10^2 & \text{drained} \end{cases} \quad (C.1)$$
$$\Pi_1 = \frac{2k}{\left(\frac{\rho_w}{\rho_s}\right) \cdot \pi \cdot g} \cdot \frac{T}{\hat{T}^2}; \quad \hat{T} = \frac{2L}{\sqrt{\frac{D+(K_f/n)}{\rho_s}}}; \quad D = \frac{E_s}{3(1-2\nu)}$$

and the parameters are,

Π_1 is the dimensionless number [-];

k is the permeability of the soil [m/s];

ρ_w is the density of water [kg/m³];

ρ_s is the density of the soil [kg/m³];

g is the gravity due to acceleration [m/s²];

T is the time period of the wave [s];

L is the drainage length [m];

K_f is the bulk modulus of the fluid [kPa];

n is the porosity of the soil [-];

E_s is the young's modulus of the soil [kPa];

ν is the Poisson's ratio [-];

Input	Value	Units
k_v	$0.0825E-3$	m/s
ρ_w	1000	kg/m^3
ρ_s	1900	kg/m^3
g	9.81	m/s
T	10	s
L	18	m
K_f	2.2	GPa
n	0.45	–
E_s	37	MPa
ν	0.2	–
D	30.83	MPa
Output	Value	Units
\hat{T}	0.071	s
Π_1	$5E-3$	–

Table C.1: Drainage type investigation

The input and the output for the wave with frequency of 0.1HZ and sand with relative density 53.95% is shown in the table C.1.

D

APPENDIX

The factors such as Relative density, load characteristics and frequency of the wave are analysed, in order to finalise the critical case. The behaviour at all the stress points is analysed but only the behaviour at stress points L and P were presented in the chapter 4. Therefore, the cyclic response in other stress points are presented in this appendix.

D.1. RELATIVE DENSITY

The cyclic response with respect to the relative density of the sand at each of the points is presented in the figureD.1. The behaviour at all the stress points is in accordance with our understanding as explained in the chapter 4 (4.3.1).

D.2. LOAD CHARACTERISTICS

The influence of load characteristics on the cyclic behaviour of the sand at each of the stress points selected for the analysis is presented in the figureD.2. The behaviour at all the stress points is in accordance with our understanding as explained in the chapter 4 (4.3.2).

D.3. WAVE FREQUENCY

The effect of wave frequency on the cyclic behaviour of the sand at each of the stress points selected for the analysis is presented in the figureD.3. The behaviour at all the stress points is in accordance with our understanding as explained in the chapter 4 (4.3.3).

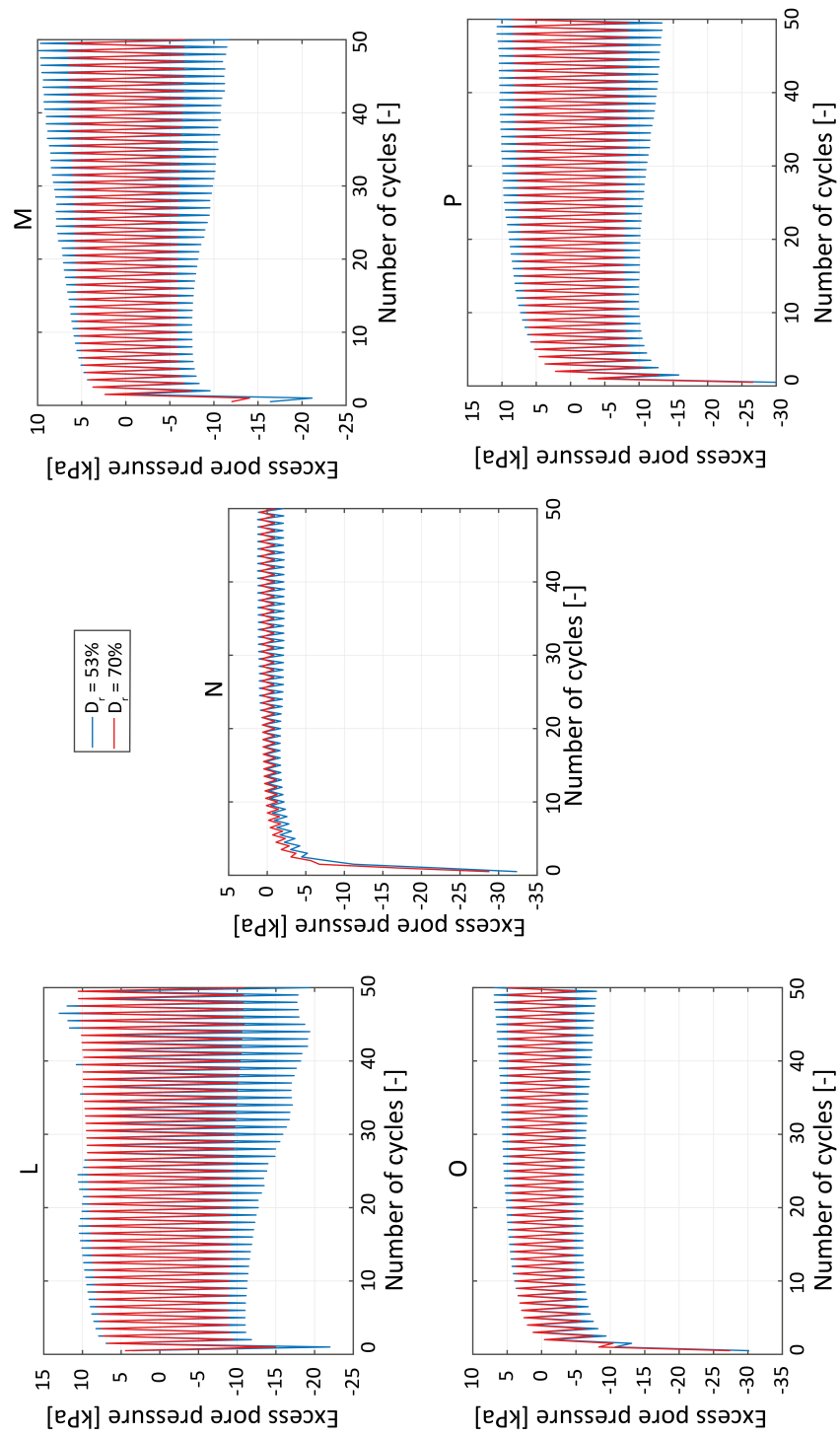


Figure D.1: Pore pressure behaviour with respect to relative density

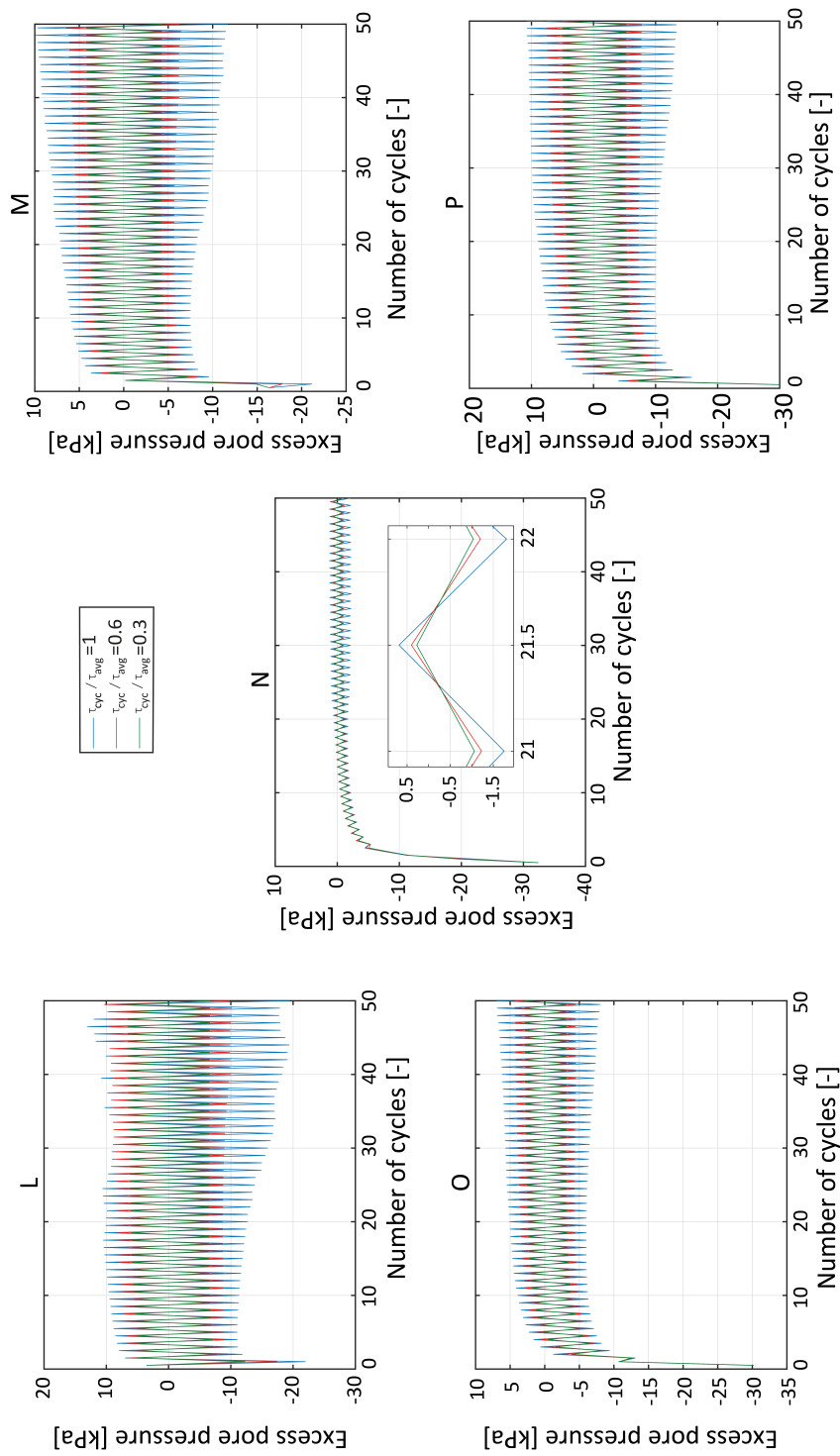


Figure D.2: The influence of load characteristics on pore pressure behaviour in response to cyclic loads

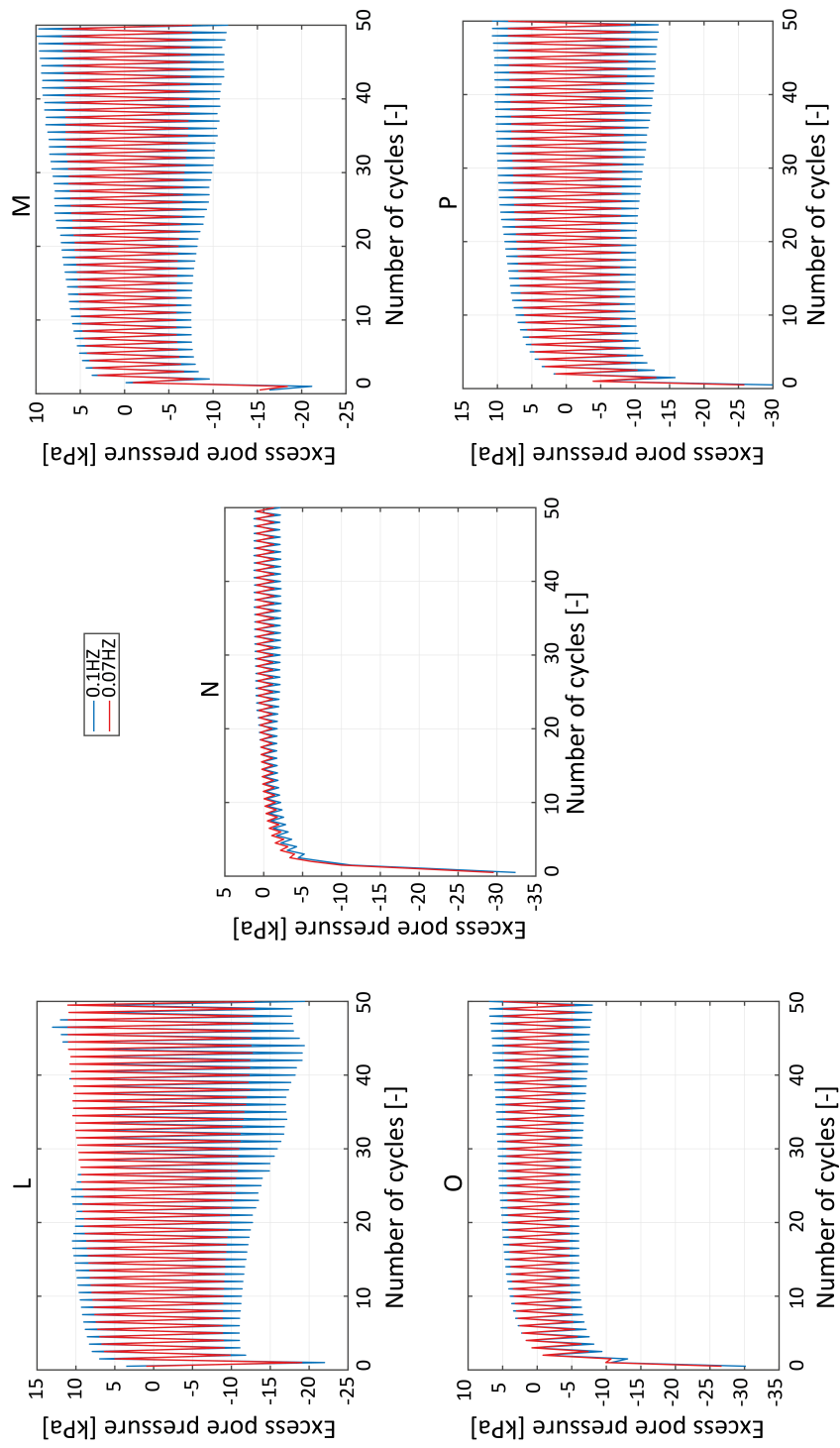


Figure D.3: The influence of frequency on pore pressure behaviour in response to cyclic loads

BIBLIOGRAPHY

- [1] Byrne.B, *Foundation design for Offshore Wind Turbines [Lecture notes]*, (2011).
- [2] DNV, *CN-30.4- Foundations*, (1992).
- [3] L. J. Prendergast, K. Gavin, and P. Doherty, *An investigation into the effect of scour on the natural frequency of an offshore wind turbine*, *Ocean Engineering* **101**, 1 (2015).
- [4] R. Brinkgreve, *Behaviour of soil and Rocks [Lecture on UBCSAND model]*, (2015).
- [5] H. Matsuoka and T. Nakai, *Relationship among Tresca, Mises, Mohr-Coulomb and Matsuoka-Nakai failure criteria*. *Soils and Foundations* **25**, 123 (1985).
- [6] G. G. I. Herle, *Determination of parameters of a hypoplastic constitutive model from properties of grain assemblies*, *Mechanics of Cohesive-frictional Materials* **4**, 461 (1999).
- [7] C. Lupea, *Long Term Effects of Cyclic Loading on Suction Caisson Foundations*, Ph.D. thesis, Delft University of Technology (2013).
- [8] M. Randolph and S. Gourvenec, *Offshore Geotechnical Engineering* (Taylor and Francis, 2011) p. 561.
- [9] S. Gourvenec, *Failure envelopes for offshore shallow foundations under general loading*, *Géotechnique* **57**, 715 (2007).
- [10] J. V. D. TEMPEL, *Design of Support Structures for Offshore Wind Turbines*, Ph.D. thesis, Delft University of Technology (2006).
- [11] T. Naves, *Cylinder island Foundation - An innovative offshore foundation*, (2013).
- [12] A. Mbistrova, *Financing and Investment trends of the European wind industry in 2016*, Tech. Rep. (Wind Europe, 2017).
- [13] DNV, *Guidelines for Design of Wind Turbines* (2002) pp. 187–221.
- [14] S. Malhotra, *Wind Turbines* (Intech, 2011) pp. 231–264.
- [15] C. Rasch, *Modelling of cyclic soil degradation*, (2016).
- [16] API, *Geotechnical and Foundation Design Considerations* (American petroleum Institute, 2011).
- [17] C. L. Bakmar, *Design of Offshore Wind Turbine Support Structures: Selected topics in the field of geotechnical engineering*, Ph.D. thesis, AALBORG UNIVERSITY (2009).
- [18] Janbu, *Settlement calculations Based on the Tangent Modulus Concept*, (1967).
- [19] K. H. Andersen, *The Third ISSMGE McClelland Lecture*, in *The Third ISSMGE McClelland Lecture* (Taylor and Francis, 2015).
- [20] T. Wichtmann, *Institut für Grundbau und Bodenmechanik*, Ph.D. thesis (2005).
- [21] K. Andersen, Knut H and Hoeg, *Deformation of soils and displacements of structures subjected to combined static and cyclic loads*, in *Proceedings of the Tenth European Conference on Soil Mechanics and Foundation Engineering* (Associazione Geotecnica Italiana, 1992).
- [22] H. Yildirim and H. Erşan, *Settlements under consecutive series of cyclic loading*, *Soil Dynamics and Earthquake Engineering* **27**, 577 (2007).
- [23] H. Taiebat and J. Carter, *Numerical studies of the bearing capacity of shallow foundations on cohesive soil subjected to combined loading*, *Géotechnique* **50** (2000).

- [24] B. Byrne, G. Houlsby, and C. Martin, *Cyclic loading of shallow offshore foundations on sand*, Int. Conf on Physical Modelling in ... , 1 (2002).
- [25] B. W. Byrne and G. T. Houlsby, *Experimental Investigations of the Response of Suction Caissons to Transient Vertical Loading*, Journal of Geotechnical and Geoenvironmental Engineering **130** (2004), 10.1061/(ASCE)1090-0241(2004)130:3(240).
- [26] G. Gottardi, G. T. Houlsby, and R. Butterfield, *Plastic response of circular footings on sand under general planar loading*, Géotechnique **49**, 453 (1999).
- [27] M. F. Bransby and M. F. Randolph, *Combined loading of skirted foundations*, Géotechnique **48**, 637 (1998).
- [28] B. Zhu, B. Byrne, and G. Houlsby, *Long-Term Lateral Cyclic Response of Suction Caisson Foundations in Sand*, Journal of Geotechnical and Geoenvironmental Engineering **139**, 73 (2013).
- [29] O. C. Zienkiewicz, C. T. Chang, and P. Bettess, *Drained, undrained, consolidating and dynamic behaviour assumptions in soils*, Géotechnique **30**, 385 (1980).
- [30] G. Gudehus, *A comprehensive constitutive equation for granular materials*, Soils and Foundations **36**, 1 (1996).
- [31] A. Petalas and V. Galavi, *Plaxis Liquefaction model UBC3D-PLM*, Tech. Rep. (PLAXIS B.V, 2013).
- [32] C. Pasten, H. Shin, and J. C. Santamarina, *Long-Term Foundation Response to Repetitive Loading*, Journal of Geotechnical and Geoenvironmental Engineering **140**, 04013036 (2013).
- [33] R. Jardine, A. Puech, and K. H. Andersen, *CYCLIC LOADING OF OFFSHORE PILES: POTENTIAL EFFECTS AND PRACTICAL DESIGN*, Proceedings of the 7th International Conference of Offshore Site Investigations and Geotechnics (2012).
- [34] P. Peralta, *Investigations on the behaviour of large diameter piles under long-term lateral cyclic loading in cohesionless soil*, Phd thesis, Leibnitz University (2010).
- [35] M. J. P. Van Wijngaarden, *Gravity based foundations for offshore wind turbines Cyclic loading and liquefaction*, Ph.D. thesis, Delft University of Technology.
- [36] J. Jonkman, S. Butterfield, W. Musial, and G. Scott, *Definition of a 5-MW reference wind turbine for offshore system development*, Contract , 1 (2009).
- [37] M. Kühn, *Dynamics and design optimization of offshore wind conversion systems*, Ph.D. thesis, Delft University of Technology (2001).
- [38] A. Niemunis, T. Wichtmann, and T. Triantafyllidis, *A high-cycle accumulation model for sand*, Computers and Geotechnics **32**, 245 (2005).
- [39] W. Fellin, *Hypoplasticity for beginners*, Institu für Geotechnik und Tunnelbau, Universitat ... , 1 (2002).
- [40] P. A. von Wolfersdorff, *Hypoplastic relation for granular materials with a predefined limit state surface*, Mechanics of Cohesive-Frictional Materials **1**, 251 (1996).
- [41] I. Niemunis, A. & Herle, *Hypoplastic model for cohesionless soils with elastic strain range*, Mechanics of Cohesive-frictional Materials (1997).
- [42] J. Long and G. Vanneste, *Effects of cyclic lateral loads on piles in sand*, Journal of Geotechnical Engineering **120**, 225 (1994).
- [43] G. Christakos, *Soil behaviour under dynamic loading conditions: Experimental procedures and statistical trends*, Stochastic Environmental Research and Risk Assessment **17**, 175 (2003).
- [44] R. Brinkgreve, *Behaviour of soil and rocks [Lecture on Hypoplastic sand]*, (2015).
- [45] R. B. J. Brinkgreve, *Reference Manual*, Plaxis Bulletin (2017).

-
- [46] M. SRBULOV, *Geotechnical Earthquake Engineering* (Springer).
- [47] J. K. Mangal, G. T. Housby, and Others, *Partially-Drained Loading of Shallow Foundations on Sand*, (1999).
- [48] NEN-EN 1997-1, *Euro code 7: Geotechnical design*, (2016).
- [49] G. Lloyd, *Regulation of the Certification of Wind Energy Conversion Systems, Rules and Regulations IV: Non Marine Technology Part 1*, Wind Energy , 1 (2005).